CCFE
CULHAM CENTRE FOR FUSION ENERGY

CCFE-PR(16)58

J-Ch. Sublet, M. Fleming, and M. Gilbert

FISPACT-II: A Modern Simulation Architecture for Inventory, Nuclear Observables and Materials Science

FISPACT-II: A Modern Simulation Architecture for Inventory, Nuclear Observables and Materials Science

J-Ch. Sublet[a], M. Fleming[a], M. Gilbert[a]

[a]UK Atomic Energy Authority, Culham Science Centre, Abingdon, OX14 3DB, UK

FISPACT-II: A Modern Simulation Architecture for Inventory, Nuclear Observables and Materials Science

J-Ch. Sublet[a,*], M. Fleming[a], M. Gilbert[a]

[a] *UK Atomic Energy Authority, Culham Science Centre, Abingdon, OX14 3DB, UK*

Abstract

The inventory code FISPACT-II, when connected to the nuclear data libraries TENDL-2015, ENDF/B-VII.1, JENDL-4.0u or JEFF-3.2, forms a simulation platform for modelling activation, transmutation processes and simulating radiation damage sources terms. The system has extended nuclear data forms, uncertainty quantification and propagation models which have been the subject of recent validation efforts including inventory simulations, fission and fusion decay heat, astrophysical nucleosynthesis. Summaries of key findings are presented and comments are made on the processes and the impacts of the major nuclear data libraries.

Keywords: Nuclear Data, Bateman, Inventory, Multi-physics, TENDL, General-purpose

Contents

1. Introduction

Knowledge of the nuclide inventory of fission and fusion reactor materials is essential for many applications. Depending on the time-scales involved, these range in fission from fuel/cladding behaviour in cycle and loss-of-coolant accidents (LOCAs) to waste classification and decommissioning processes. For fusion, these data are required for a variety of aspects including operation, maintenance planning, sensitive equipment damage and decommissioning.

The challenges of performing simulations for fusion are tremendous: higher-energy neutron reactions, an inability to pre-determine the reaction channels of importance and limited nuclear data (of sufficient quality). This has necessitated the creation of technological simulation tools which handle *all* nuclides, decays, reaction channels, isomers and tracks them with a code system designed to be as general-purpose and flexible as possible. This challenge has resulted in a powerful, modern code; FISPACT-II[1],

*Corresponding author

Email addresses: jean-christophe.sublet@ukaea.uk (J-Ch. Sublet), michael.fleming@ukaea.uk (M. Fleming), mark.gilbert@ukaea.uk (M. Gilbert)

which can access any ENDF-6 formatted nuclear data and generates a variety of un-engineered[1] outputs.

FISPACT-II is a direct replacement of the now obsolete FISPACT code, which was developed and maintained for more than 20 years [2, 3, 4] at UKAEA, and was itself based on the much earlier fission-orientated code FISPIN [5]. That system became too cumbersome and inflexible to adapt to the latest advances in nuclear physics and nuclear data, prompting the development of FISPACT-II [6] over a number of years using modern, object-style Fortran. The core of FISPACT-II is the modern LSODE [7] stiff-ode solver, which integrates the rate equations forward in time. It also uses dynamical memory allocation and so may be readily adapted to any energy group structure. It contains four major subsystems for handling (1) nuclear data reduction, (2) assembling and solving the rate equations for the inventory, (3) computing pathways and uncertainties and (4) computing and outputting derived radiological data.

The advantage of FISPACT-II is that it is not burdened by the compensations and restrictions of legacy codes. The ability to access any nuclear data and follow any target/reaction/decay on some 2809 targets and 3875 radionuclides (including all known isomeric states) allows FISPACT-II to simulate outside the proverbial box: fixed fissile systems, limited fission yields and/or reactions on the products, restrictions on incident particles, energies, emitted data, targets, decay chains and of course fixed nuclear data. To build confidence in a relatively new, modern code verification and validation is required. This has been the subject of considerable effort at the UK Atomic Energy Authority, resulting in a variety of V&V reports of which fission and fusion decay heat and inventory simulations are discussed in this paper.

2. Code Functionalities

2.1. Nuclear data reduction

The nuclear data forms provided for FISPACT-II are complex and include physics forms for a variety of simulations. In order to perform inventory and inventory-derivative simulations, the nuclear data must be reduced with incident particle, irradiation and material data into forms suitable for use in the rate equations and responses. This section describes these processes which form the foundation for the subsequent sections.

2.1.1. Reaction collapse

Before performing time-dependent simulations, FISPACT-II must generate the one-group cross sections which will be used to populate the rate equations. For this a user-supplied incident-particle spectrum must be provided in one of the group structures for which nuclear data is available. Where the data is not in a compatible energy-group structure, a group conversion can be performed by FISPACT-II.

The convolution of the incident particle spectrum ϕ_i with the multi-group cross sections σ_i on some energy group with N bins is defined as

$$\bar{\sigma} = \sum_i^N W_i \sigma_i \text{ , using weights } W_i, \quad (1)$$

$$W_i = \phi_i / \sum_i^N \phi_i. \quad (2)$$

The code accommodates energy correlations within each reaction channel, but is also designed to use cross-channel correlations when the data becomes available,

$$Cov(\bar{\sigma}_\mu, \bar{\sigma}_\nu) = \sum_{i=1}^N \sum_{j=1}^N W_i W_j Cov(\sigma_\mu, \sigma_\nu), \quad (3)$$

for $\mu \neq \nu$ with all reaction channels μ, ν. With the currently available nuclear data forms and uncertainty correlations, the variance is given by

$$var(\bar{\sigma}_\mu) = Cov(\bar{\sigma}_\mu, \bar{\sigma}_\mu) = \sum_{i,j=1}^N W_i W_j Cov(\sigma_\mu, \sigma_\mu). \quad (4)$$

These are then used to define the fractional uncertainties in each cross section as

$$\Delta_{\bar{\sigma}_\mu} = \sqrt{var(\bar{\sigma}_\mu)} / \bar{\sigma}_\mu. \quad (5)$$

These uncertainties are then used in the pathways-based uncertainty, Monte-Carlo sensitivity-uncertainty and nuclide depletion uncertainty calculations, alongside the decay and fission yield uncertainties.

FISPACT-II can process the ENDF-6 NI-type covariance data with LB=1, 5, 6 or 8. The covariance data in ENDF files are stored in energy structures which include fewer bins than the multi-groups employed by the FISPACT-II cross section data. To map the covariance data onto the cross sections a natural projection operator S_i^k is used, as shown in Figure 1, where the i index represents the energy group of the cross section, k represents the energy group of the covariance data and

$$S_i^k = \begin{cases} 1 & \text{if bin } i \in \text{bin } k \\ 0 & \text{otherwise} \end{cases} . \quad (6)$$

2.1.2. Decay processes

FISPACT-II reads directly from the `MF`=8, `MT`=457 decay data in the ENDF-6 format, considering 27 different decay modes as summarised in Table 1. In decay processes the Δ values indicate the modification of the parent

[1] As compared with industry-standard codes which (as is proper) include many compensations to ensure accurate results irrespective of limitations in nuclear data, technological barriers or lack of physics knowledge.

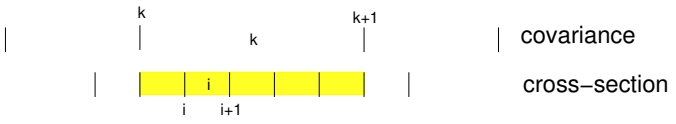

Figure 1: (Colour online) Projection operator S_i^k maps cross-section energy bins to covariance energy bins. The shaded energy bins have $S_i^k = 1$, and all others have $S_i^k = 0$.

nuclide, while additional secondary particles are also introduced into the inventory calculation, including ^{1}H and ^{4}He. Spontaneous fission may be treated simply as a disappearance of the parent, or fission yield data from `MF`=8, `MT`=454 or `MT`=459 may be read from the provided nuclear data libraries and used to track the inventories of these nuclides. Note that in some files the normalisation method used to match the sum of partial decay pathways with a well-known half-life is provided by the `RTYP`=10 'unknown' channel.

Emitted particle spectra are essential for many applications with γ spectra being an important case. FISPACT-II reads the `MF`=8 `MT`=457 data for emitted energy information, taking the following:

- **decay heating** – The average decay energies for light particles, electromagnetic radiation and heavy particles. These are used to calculate the beta, gamma and alpha decay heat values.
- **gamma spectra** – The discrete line energies, intensities and normalisation factors from `STYP`=0,9 are used to generate energy contributions which are added into a corresponding bin of a multi-group structure.

For any of the available group structures in FISPACT-II, the product of the line intensity I, energy E and a normalisation factor fd or fc are added to the energy group containing E, for each of the lines available in the decay data. Where there is *no spectral data* in the file, but average energy release values are provided, FISPACT-II can generate an approximated spectrum. This is necessary to assess gamma responses, such as dose rate, which cannot be calculated without some spectral information or an equivalent approximation.

For the approximation, a maximum γ energy (E_m) is assumed based on the values of Table 2.

The intensity used to calculate the contribution in each group of the spectrum is then

$$I_i = \frac{a\langle\gamma\rangle}{E_m}\left(\frac{e^{-a\eta_{i-1}} - e^{-a\eta_i}}{1-(1+a)e^{-a}}\right), \tag{7}$$

where $\eta_i = E_i/E_m$ and a is an arbitrary constant set to 14.

The bremsstrahlung radiation from high-energy β-decays may also be significant, particularly where the total γ activity is small. The method employed by FISPACT-II is based on the approach of Jarvis [8], but extended from mono-energetic electrons to use the average from a continuous spectrum and with an average nuclear charge from the full isotopic material mixture.

2.1.3. Fission yields

Fission yields may be used for any nuclides with ENDF-6 fission yield files. This includes neutron-induced fission as well as spontaneous fission and charged-particle-induced fission yields from protons, deuterons, alphas and γ-rays. For particle-induced fission, the energy dependence of the yields are determined from a projection operation similar to that used in covariance projection, as shown in Figure 1. For a particle-induced fission yield file with data for energies E_i, $i \in [1, n]$, the group boundaries between different energies are defined as the mid-points, for each group the maximum energy for each fission yield group g_i is:

$$E_{max}(g_i) = \frac{E_{i+1} - E_i}{2} \quad \forall i \in [1, n-1]\,. \tag{8}$$

The projection operator S_i^j of Equation 6 can then be applied from the cross section group index i of the incident-particle spectrum onto the fission yield group j. The weights for the fission yield are calculated using the energy-dependent reaction rate weighting:

$$W_j = \frac{1}{\phi\sigma}\sum_{i=1}^{N} S_i^j \phi_i \sigma_i, \text{ where} \tag{9}$$

$$\phi\sigma = \sum_{i=1}^{N} \phi_i \sigma_i. \tag{10}$$

The spectrum-weighted fission yield for each nuclide, indexed by μ, is then

$$Y_\mu = \sum_{j=1}^{n} W_j Y_{\mu,j}. \tag{11}$$

FISPACT-II can use either the independent or cumulative fission yields from `MF`=8, `MT`=454 ot 459, respectively. The set of fissile nuclides whose fissions are fully modelled with the yields can be specified as any subset of the full range (potentially more than 100 with GEFY).

2.1.4. Charged-particle irradiations

By keeping FISPACT-II open to all ENDF-6 nuclear data files, it naturally handles charged-particle-induced reactions and can be used to simulate charged-particle irradiation scenarios with all of the same code features used in neutron irradiation. This requires the nuclear data for charged-particle interactions, for which there are a few libraries to draw upon. TENDL provides complete data for proton, deuteron, alpha and γ-ray incident reactions and the most recent TENDL libraries are processed and distributed with the standard code package.

Unlike at low energies, where individual channels such as (z,p), (z,α), (z,γ), etc. are well defined, at high energies

Table 1: Decay Types (MF=8, MT=457) recognised by the code. The column labelled 'Code' is the description used in output from FISPACT-II, NSEC is the number of secondaries and 'Secs' is an abbreviation for 'Secondaries'.

IRT	RTYP	Description	ΔZ	ΔA	Code	NSEC	Secs
1	1	β^- decay	1	0	b-	0	
2	2	β^+ decay or electron capture	−1	0	b+	0	
3	3	isomeric transition (IT)	0	0	IT	0	
4	4	α decay	−2	−4	a	1	^{4}He
5	5	neutron emission	0	−1	n	0	
6	6	spontaneous fission (SF)	−999	−999	SF	0	
7	7	proton emission	−1	−1	p	1	^{1}H
8	8	not used	0	0	0		
9	9	not used	0	0	0		
10	10	unknown	0	0	0		
11	1.5	β^- decay + neutron emission	1	−1	b-n	0	
12	1.4	β^- decay + α emission	−1	−4	b-a	1	^{4}He
13	2.4	β^+ decay + α emission	−3	−4	b+a	1	^{4}He
14	2.7	β^+ decay + proton emission	−2	−1	b+p	1	^{1}H
15	3.4	IT followed by α emission	−2	−4	IT+a	1	^{4}He
16	1.1	double β^- decay	2	0	b-b-	0	
17	1.6	β^- decay followed by SF	−999	−999	b-SF	0	
18	7.7	double proton emission	−2	−2	pp	2	^{1}H ^{1}H
19	2.2	double β^+ or electron capture	−2	0	b+b+	0	
20	1.55	β^- and double neutron emission	1	−2	b-2n	0	
21	1.555	β^- and triple neutron emission	1	−3	b-3n	0	
22	1.5555	β^- and quadruple neutron emission	1	−4	b-4n	0	
23	5.5	double neutron emission	0	−2	2n	0	
24	5.55	triple neutron emission	0	−3	3n	0	
25	2.77	β^+ decay + double proton emission	−3	−2	b+2p	2	^{1}H ^{1}H
26	2.777	β^+ decay + triple proton emission	−4	−3	b+3p	3	^{1}H ^{1}H ^{1}H
27	2.6	β^+ decay followed by SF	−999	−999	b+SF	0	

Table 2: Maximum γ energies for various decay modes.

Decay mode	E_m
β^-	$2\langle\beta\rangle$
β^+	5 MeV
α	0
Isomeric transition	$\langle\gamma\rangle$

the distinguishing of channels such as (z,3n2p) from (z,nα) or (n,2npd) is not meaningful from an inventory perspective (and not believable from a nuclear data perspective). For all TENDL data above 30 MeV, including the neutron and charged-particle files, the use of total (heavy and light) residual production cross sections offers complete information for the radionuclide yields from nuclear reactions – the fundamental data for inventory calculations. These include spallation-evaporation reactions and associated yields, as shown in the yields for ^{120}Sn in Figure 2. These are all processed as a (n,O) reactions by FISPACT-II and populate all of the residual production channels in the rate equations.

2.2. Inventory calculation

Following the reduction of the nuclear data and user-supplied irradiation conditions, FISPACT-II builds the rate equations [9]:

$$\frac{dN_i}{dt} = \sum_j (\lambda_{ij} + \phi(t)\sigma_{ij})N_j \,, \tag{12}$$

where

N_i = number of nuclide i at time t
ϕ = total projectile flux (cm^{-2}s^{-1})

(for $j \neq i$):
λ_{ij} = decay constant of nuclide j producing i (s^{-1})
σ_{ij} = cross section for reactions on j producing i (cm^2)

(for $j = i$):
$\lambda_j = -\lambda_{jj}$ = total decay constant of nuclide j (s^{-1})
$\sigma_j = -\sigma^{jj}$ = total cross section for j (cm^2).

Cross sections and decays may include the full fission yields if particle-induced and spontaneous fission are included.

The code execution sequence begins with a set of initial physical conditions and then progresses through some irradiation or sequence of irradiation steps, followed by zero-

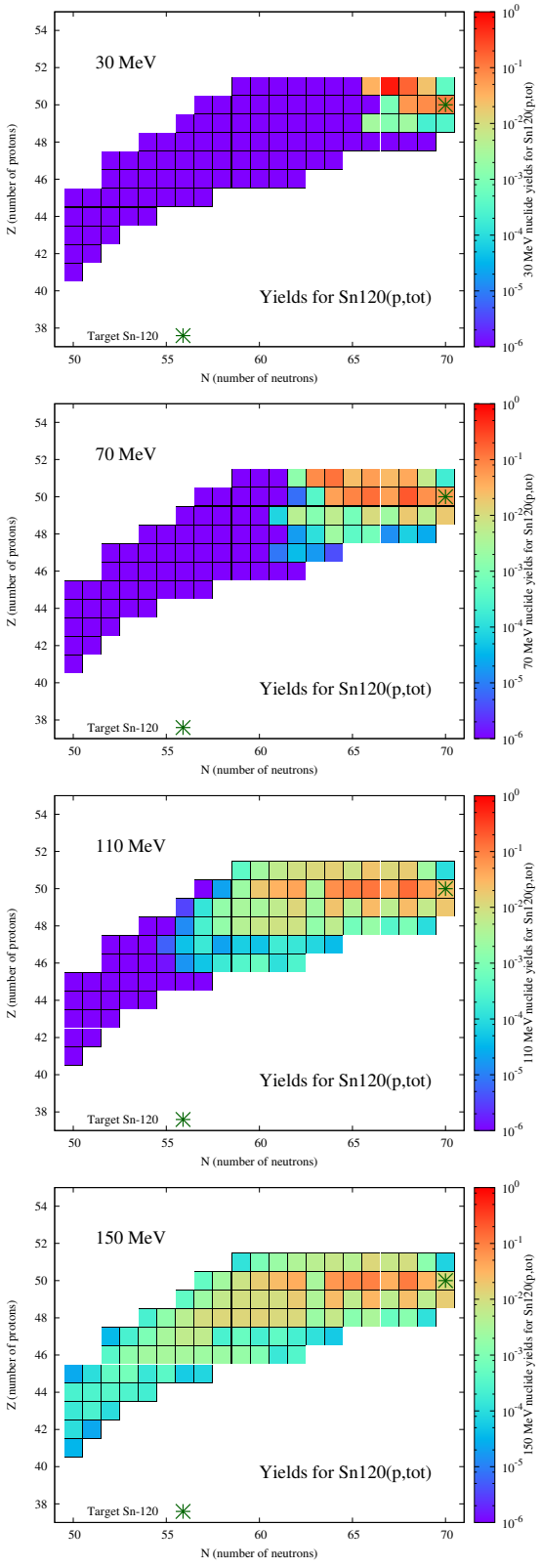

Figure 2: TENDL-2015 total residual nuclide production cross sections from proton-induced reactions on ^{120}Sn. Incident energies for 30, 70, 110 and 150 MeV are shown to demonstrate the range of yields over 30-200 MeV.

flux cooling stages, outputting requested data throughout the calculation.

2.2.1. Rate equation solution

FISPACT-II uses the well-established LSODE solver [7, 10, 11] written at Lawrence Livermore Laboratory, wrapping it within a modern Fortran module to dynamically allocate arrays, but without any significant modifications to the solver itself. LSODE uses backward differentiation, known as Gear's method, employing a series of solver-internal timesteps. LSODE calculates the inventories N_i and local error estimates e_i for each of the X nuclides, which are used to define a single error test value $\mathcal{E}$

$$\mathcal{E} = \left(\frac{1}{X} \sum_{i=1}^{X} \frac{e_i}{w_i} \right)^{1/2} , \text{ where} \quad (13)$$

$$w_i = rtol\, N_i + atol\,. \quad (14)$$

The solution algorithm will finish when the criterion $\mathcal{E} \leq 1$ is met. The relative `rtol` and absolute `atol` tolerances may be set by the user, allowing convergence tests for sensitive simulations.

2.2.2. Multi-step irradiation

FISPACT-II uses two normalisation methods, either through user specification of the incident particle flux (in cm^{-2} s^{-1}) or through a volumetric power rating (in W cm^{-3}). The power normalisation uses the full kinetic energy release per mass (KERMA) data from the nuclear data, with options to select total or any combination of partial KERMA values (for example, fission, capture, absorption, inelastic, etc.). Particularly in reactor simulations where the neutron flux varies over time with a constant power rating, the use of power normalisation is not only more simple, but necessary when reactor simulations are separated by many MWd per tonne. To maintain a constant power normalisation, the use of built-in steped irradiation scenarios allows the user to renormalise on a specified set of time-steps.

Besides normalisation alterations during the simulation, the incident particle spectrum may be modified with a recalculation of the particle-induced cross sections, self-shielding factors, fission yield weightings and the corresponding changes to the secondary data such as KERMA. This allows the power normalisation to be fit to a fully time-dependent set of spectra and material composition, with the associated changes in self-shielding and KERMA. Cooling-only simulation and multi-projectile simulation may also be performed.

2.3. Self-shielding corrections

FISPACT-II provides two methods for resonance self-shielding corrections, through the probability table (PT) methods provided by CALENDF-generated PTs for each of the multi-group nuclear data libraries or the 'Universal Curve Model' for geometry-specific self-shielding in thin and thick targets.

2.3.1. Probability tables

Keywords in the FISPACT-II `input` file may be used to cause probability table sub-group data generated by CALENDF [12, 13] to be used to model dilution effects in the computation of the collapsed effective cross sections. CALENDF [14] provides data in five sets of macro-partial cross sections; the CALENDF set macro-`MT` numbers (cal-mt) are defined in Table 3. The sum of these macro-partial cross sections gives the total cross section in each energy group over the resonance regions covered.

Table 3: CALENDF macro-`MT` number.

cal-mt	Description	`MT` in set
2	elastic scattering	2
101	absorption (no outgoing neutron)	102 103 107
18	fission total	18
4	inelastic scattering (emitting one neutron)	4 11
15	multiple neutron production (excluding fission)	5 16 17 37

The data provided by CALENDF are effective cross-section σ and probability values P depending on four parameters:

$$\sigma(x,n) \equiv \sigma(p,g,x,n) \quad (15)$$

$$P(x,n) \equiv P(p,g,x,n)\,, \quad (16)$$

where
p = parent nuclide number,
g = energy group number,
x = macro-partial (or total) index, and
n = quadrature index.

In the expressions below, we suppress the explicit display of dependence of cross section on the parent nuclide p and energy group g except in the formulae for dilution. The infinite dilution ($d = \infty$) cross section for a given parent, energy group and component is

$$\begin{aligned}\sigma(x,d=\infty) &= \frac{1}{E_{max}-E_{min}}\int_{E_{min}}^{E_{max}}\sigma(E)\,dE \\ &= \sum_{n=1}^{N} P(x,n)\sigma(x,n)\,. \end{aligned} \quad (17)$$

When a nuclide is a part of a homogenous mixture of nuclides, then the effective cross sections in the resonance regions are reduced, and are parameterised using the dilution cross section d [15, 16, 17, 12]:

$$\sigma(x,d) = \frac{\sum_{n=1}^{N} P(x,n)\sigma(x,n)/(\sigma_t(n)+d)}{\sum_{n=1}^{N} P(x,n)/(\sigma_t(n)+d)}\,, \quad (18)$$

where the total cross section is given by the sum of the macro-partials:

$$\sigma_t(n) = \sum_{x=1}^{X}\sigma(x,n)\,. \quad (19)$$

The total cross section for nuclide p in energy group g at dilution d is given by

$$\sigma^{tot}(d) = \sum_{x=1}^{X}\sigma(x,d_p)\,. \quad (20)$$

The probability table data from CALENDF are used in conjunction with the 709 and 1102 group data in the ENDF-6 libraries. In the following discussion, we use the term 'library' or 'LIB' to refer to either the TENDL or alternative ENDF-6 forms as appropriate. The dilution computed using the CALENDF data is applied either as scaling factors to the library cross-section data or as replacements over the energy ranges for which the probability table data are available. The scaling or replacement approach partial or total scaling may be selected by user input.

Scaling applied to LIB data:. Scaling is applied to the library data in one of two ways depending on user input. If the partial self-shielding scaling factor option is chosen, then the cross section for nuclide p in energy group g and for `MT` value y belonging to the macro-partial group x is scaled according to

$$\sigma^{new}(y,d) = \sigma^{LIB}(y)\left(\frac{\sigma(x,d)}{\sigma(x,d=\infty)}\right) \quad (21)$$

and for the total scaling factor

$$\sigma^{new}(y,d) = \sigma^{LIB}(y)\left(\frac{\sigma^{tot}(d)}{\sigma^{tot}(d=\infty)}\right)\,. \quad (22)$$

The dilution $d(p,g)$ for a given nuclide p and energy group g is computed using a weighted sum over all the nuclides, $q \in [1,Q]$ in the mixture. The fraction of nuclide q in the mixture is f_q. Nuclides in the mixture may or may not be included in the list of nuclides to which the self-shielding correction is to be applied. Nuclides to which self-shielding corrections are applied must be in the mixture list. The first approximation is given using the total cross sections from the cross-section library:

$$d^{(0)}(p,g) = \sum_{\substack{q=1\\ p\neq q}}^{Q}\frac{f_q\sigma^{LIB-tot}(q,g)}{f_p}\,, \quad (23)$$

where

$$\sigma^{LIB-tot}(p,g) = \sum_{y}\sigma^{LIB}(p,g,y)\,. \quad (24)$$

Over the energy range for which the probability table data are available for those nuclides in the mixture for which self-shielding corrections are being applied, the approximation given by Equation 23 is iteratively refined

using

$$S^{(i)}(g) = \sum_{q=1}^{Q} f_q \sigma^{LIB-tot}(q,g) \times \left(\frac{\sigma^{tot}(q,g,d^{(i)}(q,g))}{\sigma^{tot}(q,g,\infty)} \right) \quad (25)$$

$$d^{(i+1)}(p,g) = \frac{S^{(i)}(g)}{f_p} - \sigma^{LIB-tot}(p,g) \times \left(\frac{\sigma^{tot}(p,g,d^{(i)}(p,g))}{\sigma^{tot}(p,g,\infty)} \right) . \quad (26)$$

Replacement of LIB data:. If there is only one reaction MT in the CALENDF macro-partial group, then the replacement formulae would be given by replacing the σ^{LIB} values in the above equations by the infinite dilution cross sections obtained from the CALENDF data. When there is more than one reaction in the macro-partial set, then the dilution effect has to be apportioned according to the LIB reaction cross sections.

If the partial self-shielding scaling factor option is chosen, then the cross section for nuclide p in energy group g and for MT value y belonging to the macro-partial group x is given by

$$\sigma^{new}(y,d_p) = \sigma(x,d_p) \left(\frac{\sigma^{LIB}(y)}{\sum_{y' \in x} \sigma^{LIB}(y')} \right) \quad (27)$$

and for the total scaling factor

$$\sigma^{new}(y,d_p) = \sigma(x,\infty) \left(\frac{\sigma^{LIB}(y)}{\sum_{y' \in x} \sigma^{LIB}(y')} \right) \times \left(\frac{\sigma^{tot}(d_p)}{\sigma^{tot}(\infty)} \right) . \quad (28)$$

The initial values of the dilutions are given by Equations 23 and 24 and the iterative refinements where CALENDF probability table data are available are given by

$$S^{(i)}(g) = \sum_{q=1}^{Q} f_q \sigma^{tot}(q,g,d^{(i)}(q,g)) \quad (29)$$

$$d^{(i+1)}(p,g) = \frac{S^{(i)}(g)}{f_p} - \sigma^{tot}(p,g,d_p^{(i)}) . \quad (30)$$

The set of nuclides for which the self-shielding correction is calculated and the set of nuclides included in the mixture for computing the dilution cross section is specified user input. User input also allows the values of dilution given by Equation 26 or 30 to be overridden by user-supplied dilution values.

The default method of computing self-shielding using the probability table method is to use Equations 23 and 24 for initial values, Equation 27 for cross section and iterate dilution using Equations 29 and 30. When the iteration is complete, the new collapsed cross sections are computed by applying the ssf to produce the effective cross sections. The effective self-shielding factor ssf for the collapsed cross section is given by

$$ssf(p,y) = \frac{\sigma^{new}(p,y)}{\sigma^{LIB}(p,y)} . \quad (31)$$

The self-shielding factors may be applied wherever probability table data is provided and can be used to correct specific sets of reaction rates for desired nuclides, for example the energy-dependent self-shielding factors applied to the ^{238}U neutron capture in a typical PWR spectrum and fresh fuel composition, which is shown in Figure 3. These can be updated during irradiation, accommodating changes in both nuclide inventory and spectra to alter the dilutions and reaction rates, respectively.

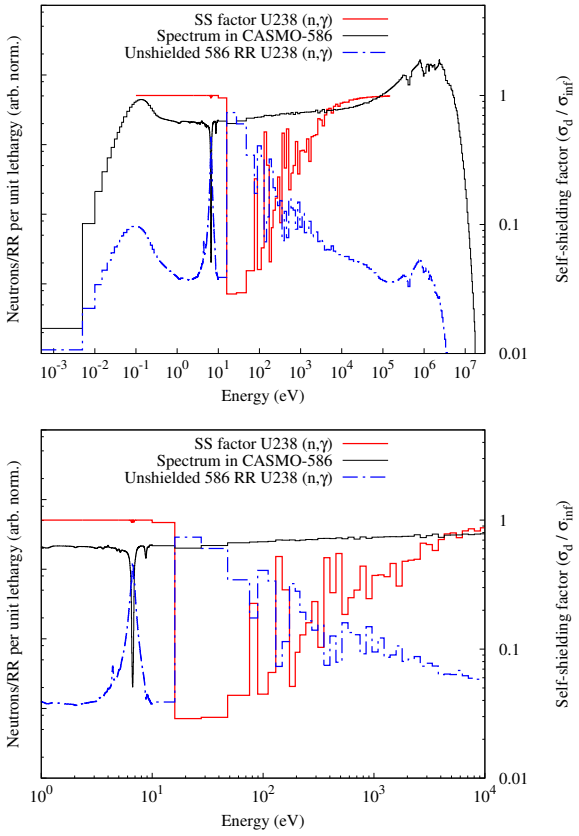

Figure 3: (Colour online) Neutron spectrum, the unshielded ^{238}U(n, γ) cross section and the energy-dependent probability table self-shielding factors calculated for the fresh fuel composition in FISPACT-IIusing ENDF/B-VII.1. Global and zoomed-in plots are provided. The integrated self-shielding factor for this cross section is 0.18.

2.3.2. Universal Curve Model

FISPACT-II provides a second method of accounting for self shielding in thin/thick targets with a variety of geometries. This can be used as an alternative to the probability table method described in the previous section which is appropriate for geometry relevant self-shielding effects.

It is not possible to use both descriptions of self shielding simultaneously.

In a series of papers [18, 19, 20], the authors Martinho, Gonçalves and Salgado described a "universal sigmoid curve" model of self shielding to account for the reduction of the neutron flux by cross section resonances in the context of neutron activation analysis. They based their development on earlier experimental and theoretical work by Baumann [21].

The Martinho et al [18] model initially described the effect of a single resonance peak in a pure target consisting of a single nuclide. The self-shielding factor G_{res} is approximated as a simple function of a single dimensionless length parameter that depends on the physical size and shape of the target as well as the peak cross section at the resonance and the resonance widths for elastic scattering and radiative capture. The final form of the model [20] accommodates a group of isolated resonances of a pure target, and the target geometry could be a foil, wire, sphere or cylinder of finite height. This model has been generalised further and applied to the mixture of nuclides required for a FISPACT-II calculation.

FISPACT-II user input invokes this model of self shielding and defines the type and dimensions of the target, as detailed in Table 4.

Table 4: Target geometry recognised by FISPACT-II.

ID	Type	Dimension(s)	Effective length (y)
1	foil	thickness (t)	$y = 1.5t$
2	wire	radius (r)	$y = 2r$
3	sphere	radius (r)	$y = r$
4	cylinder	radius (r), height (h)	$y = 1.65rh/(r + h)$

The initial form of the model [18] that accounts for the effect of a single resonance in a pure target containing a single nuclide defines a dimensionless parameter,

$$z = \Sigma_{tot}(E_{res}) y \sqrt{\frac{\Gamma_\gamma}{\Gamma}}, \tag{32}$$

that depends on the physical length y, the macroscopic cross section $\Sigma_{tot}(E_{res})$ at the energy E_{res} of the resonance peak, the resonance width Γ_γ for radiative capture and the total resonance width Γ. Then the self-shielding factor is

$$G_{res}(z) = \frac{A_1 - A_2}{1 + (z/z_0)^p} + A_2 \tag{33}$$

where the parameters defining this "universal sigmoid curve" are

$$A_1 = 1.000 \pm 0.005\,, \tag{34}$$
$$A_2 = 0.060 \pm 0.011\,, \tag{35}$$
$$z_0 = 2.70 \pm 0.09\,, \tag{36}$$
$$p = 0.82 \pm 0.02\,. \tag{37}$$

These parameters were determined empirically by Martinho et al [18] by fitting to a set of points generated by performing Monte-Carlo simulations with the MCNP code for a variety of targets of different shapes, sizes and compositions. Six nuclides that exhibit strong resonances were used individually, not as mixtures.

The model was then extended by Martinho et al [19], who defined an effective length y for cylinders of finite height, but a more significant extension was provided by Salgado et al [20], who defined an average $\langle G_{res} \rangle$ by assigning weights to each resonance and forming an average of the individual G_{res} factors calculated for each resonance individually. The weight of resonance i is

$$w_i = \left(\frac{\Gamma_\gamma}{E_{res}^2} \cdot \frac{g\Gamma_n}{\Gamma} \right)_i , \tag{38}$$

where

Γ_n is the neutron scattering width;

g is the statistical factor, $(2J + 1)/(2(2I + 1))$;

J is the spin of the resonance state;

I is the spin of the target nucleus.

Then the effective self-shielding factor is

$$\langle G_{res} \rangle = \frac{\sum_i w_i G_{res}(z_i)}{\sum_i w_i}\,. \tag{39}$$

where each z_i is calculated from Eq. 32 using the effective length of the target, y and the resonance parameters for resonance i.

This model has been generalised further in two ways to make it suitable for application in FISPACT-II. First, the average self-shielding factor is computed from the resonance parameters given in the resolved resonance range defined in the ENDF-6 `MF=2` data for a subset of the nuclides selected by user input. It is assumed that the resonances for the mixture of nuclides are separated in energy sufficiently for them not to overlap significantly.

Note that the TENDL data use a unique approach to create parameters for resolved statistical resonances for a large number of isotopes that did not have any. This method invokes global average parameters from the different systematics and from the TALYS reaction code [22]. These parameters are then used by either the CALENDF code or by the R-matrix code AVEFIT. Statistical resonance parameters are then obtained from zero up to the first excited level, reflecting the average resonance parameters coming from compound model calculations. Above the first inelastic level, grouped inelastic cross sections with local fluctuations are obtained. This method complements the measured resonance parameters, or provides a resolved resonance range when measurements do not exist. In between these two cases, statistical resonance parameters are adjusted to integral measurements when available. This method, which has been successfully applied to all isotopes living longer than one second, has been used to populate the resonance ranges of the TENDL libraries [23].

The cross section at a resonance peak is not supplied in the ENDF data. The simple expression provided by Fröhner [Eq. (186)][24] is used to supply this information.

Secondly, $\langle G_{res} \rangle$ is made energy dependent by taking averages separately for each energy bin used for the group-wise cross sections, including only those resonances with peaks in the relevant energy bin. Then this array of energy-dependent self-shielding factors is applied to each energy-dependent cross section before the cross section collapse.

The principle underlying this model of self shielding is that the resonances perturb the spectrum of the applied neutron flux. Consequently, the self shielding factors should modify the cross sections for all reactions. However, the effect of self shielding varies from reaction to reaction because of the differing energy dependencies of the cross sections.

2.4. Uncertainty quantification and propagation

Uncertainty quantification and propagation are handled through three different methods within the FISPACT-II code, including pathways-based metrics, depletion and Monte-Carlo sensitivity uncertainty. These have been complemented by Total Monte-Carlo sampling methods using GEF-based fission yields and parameter-perturbed TENDL [25, 26].

2.4.1. Pathways-based uncertainty

The default uncertainty method within FISPACT-II utilised a novel pathway algorithm [27] to identify each combination of reactions and/or decays which lead from the initial material inventory to any of the nuclides produced through irradiation. The uncertainties in each pathway are calculated from the combination of uncertainties in each reaction rate and half-life.

For all of the inventory-derived quantities Q which include contributions from multiple nuclides with individual quantities q_i, the total $Q = \sum_i q_i$ has an uncertainty

$$(\Delta Q)^2 = \sum_i \left(\frac{\Delta N_i}{N_i} \right)^2 q_i^2. \tag{40}$$

For each of the nuclide produced in the irradiation, FISPACT-II performs a search for all pathways which lead to the production of that nuclide. For each element p of the set of these pathways $\mathfrak{p}$, there exists some chain of nuclides connected by R reactions and D decays. The uncertainties in these are given by the fractional uncertainties calculated from covariance collapse $\Delta\sigma$, as in Equation 5 and the fractional uncertainties of half-lives $\Delta\tau$. The uncertainty of each pathway is calculated as

$$\left(\frac{\Delta N_{i,p}}{N_{i,p}} \right)^2 = \sum_{r \in p} \left(\frac{\Delta \sigma_r}{\sigma_r} \right)^2 + \sum_{d \in p} \left(\frac{\Delta \tau_d}{\tau_d} \right)^2 \tag{41}$$

and the total uncertainty is then

$$(\Delta N_i)^2 = \sum_{p \in \mathfrak{p}} (\Delta N_{i,p})^2 . \tag{42}$$

These uncertainties are printed for all dominant nuclides and used for the calculation of response uncertainties in Equation 40. Multi-pulse irradiations are handled by replacing the reaction uncertainties by pulse-averaged values. FISPACT-II is engineered to accommodate channel-channel and fission yield covariances, although at present the nuclear data forms available do not include the required information.

2.4.2. Depletion uncertainty

A new functionality for uncertainty quantification in nuclide depletion has been added after the 3-10 code version. While pathways-based uncertainty handles the *production* of radionuclides for the purposes of quantifying uncertainty in radiological quantities, the uncertainty in the depletion of any nuclide – whether through reactions or decays – adds an additional contribution to uncertainty propagation. In comparison with the myriad of possible pathways which produce a nuclide, the depletion occurs only through an easily classed subset of reactions which are precisely the negative diagonal terms of the rate equation matrix.

A nuclide generally may have some combination of creation and destruction,

$$\frac{dN}{dt} = -\mathsf{D}N + \mathsf{C}, \tag{43}$$

where D is a specific rate while C is a rate of creation, i.e. units of s^{-1} and atoms/s, respectively. While C typically depends on a many quantities including potentially many inventories, decays and reactions, it can be determined by direct reference to the rate equation solutions and the depletion term.

The creation terms in turn have their own associated uncertainties and are the subject of the pathways-based uncertainty analysis in FISPACT-II. To address the depletion uncertainty, FISPACT-IIconsiders three variables with their uncertainties:

$$\begin{aligned} \lambda &= \text{total decay rate for the target nuclide} \\ \Phi &= \text{flux amplitude} \\ \sigma &= \text{total non-scattering cross-section} \end{aligned}$$

The depletion specific rate $\mathsf{D} = \lambda + \Phi\sigma$, so using the standard identities for variance of sums or products of random variables we obtain:

$$\begin{aligned} var(\mathsf{D}) \quad = \quad & var(\lambda) + \Phi^2 var(\sigma) + \sigma^2 var(\Phi) \\ & + var(\sigma) var(\Phi). \end{aligned} \tag{44}$$

FISPACT-IIcalculates the fractional uncertainties for half-lives, Δ_λ, and for collapsed cross sections, Δ_σ, which are defined as $\Delta_X = \sqrt{var(X)}/X$. The estimator for the fractional error in the specific rate D is therefore:

$$\Delta_{\mathsf{D}} = \frac{1}{\mathsf{D}} \sqrt{(\lambda\Delta_\lambda)^2 + (\sigma\Phi)^2 ({\Delta_\sigma}^2 + {\Delta_\Phi}^2 + \Delta_\sigma \Delta_\Phi)}. \tag{45}$$

While FISPACT-II is designed to accommodate the uncertainties (including covariances) of incident particle spectra, the current implementation only considers uncertainties in the total flux. Note that a complete covariance treatment of the reaction rate due to cross section energy correlations is implemented, i.e. for a reaction rate R we sum over all energy groups:

$$var(R) = \sum_i \sum_j \phi_i \phi_j cov(\sigma_i, \sigma_j). \quad (46)$$

FISPACT-II outputs the specific depletion rate as well as the percent uncertainty from the equations above. These are also given as a depletion rate using the initial nuclide inventory for each step, as well as a first-order integrated value for the depletion and its uncertainty as a fraction of the final inventory. Note that this is the integrated uncertainty (in atoms) of depletion, which will grow (unbound) monotonically as a percent in pure depletion cases.

In scenarios where a nuclide may be both created and depleted - for example plutonium in a fission reactor, minor actinides, fission products, etc., a combination of both depletion and breeding uncertainties are required. To avoid the complexities and expense of full Monte-Carlo sensitivity-uncertainty analyses, FISPACT-II can be used to calculate depletion and breeding rates with uncertainties. These can be coupled with multiple different approximations. For example, the simplified piece-wise constant equations for a target nuclide of Eq. 43.

If we assume that these terms are constant over the time interval, the solution for this simplified differential equation is simply

$$N_{i+1} = \frac{\mathsf{C}_i}{\mathsf{D}_i} + \left(N_i - \frac{\mathsf{C}_i}{\mathsf{D}_i} \right) \exp\left(-\mathsf{D}_i \Delta t_i\right), \quad (47)$$

and the first order Taylor expansion of the propagated uncertainty yields:

$$\Delta {N_{i+1}}^2 = \left(\frac{\partial N_{i+1}}{\partial \mathsf{D}_i} \right)^2 \Delta {\mathsf{D}_i}^2 + \left(\frac{\partial N_{i+1}}{\partial \mathsf{C}_i} \right)^2 \Delta {\mathsf{C}_i}^2. \quad (48)$$

provides an uncertainty estimate. These methods have been tested with FISPACT-II to generate coupled uncertainties in simulated actinide inventories for fission fuels, as in Fig. 4. These rely upon complete uncertainty data, including the resolved resonance ranges, which are still incomplete in the current nuclear data sets.

2.4.3. Monte-Carlo sensitivity-uncertainty

FISPACT-II contains a Monte-Carlo sampling system for sensitivity-uncertainty analyses. Using a set of independent variables which are cross sections σ_i or half-lives τ_i, with their associated distributions, means and first moments, FISPACT-II will perform a series of inventory calculations with sampled values for those independent variables. From these sampled calculations, targeted responses variables Q_i, which may include nuclide inventories or responses. Energy covariances within each reaction rate are handled by the nuclear data collapse and incorporated into the distributions of the cross sections, but channel to channel correlations can be handled as well. This is handled by calculating a similarity transform to diagonalise the channel-to-channel covariance matrix and sample from the diagonal variables and their distributions.

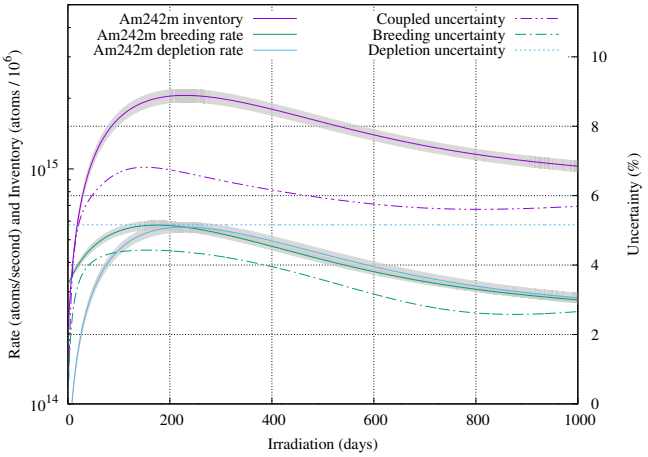

Figure 4: (Colour online) Coupled breeding-depletion uncertainty analysis of Am242m inventory in a PWR MOX spectrum with constant neutron flux of 1.0E+14 n cm^{-2} s^{-1}. The **DEPLETION** uncertainty is constant for this single incident particle spectrum simulation, while breeding paths and their combined uncertainties are time-dependent.

Distributions may be selected from log-normal (default), normal, uniform or log-uniform. The calculations can be performed with any combination of irradiation scenarios allowable within FISPACT-II and in all calculations the Pearson correlation coefficients between the independent and dependent variables are calculated and output.

2.5. Primary damage response functions or PKAs

While the core functionality of FISPACT-II is still guided by nuclear (fusion or fission) operational, maintenance planning, decommissioning, and waste concerns, which necessarily requires accurate predictions of radiological responses, the FISPACT-II team is also mindful of opportunities to exploit the FISPACT-II infrastructure to provide useful data for other communities. This has already led to the FISPACT-II output including gas production, kerma, and displacement-per-atom (dpa) values for every irradiation step, as well as the time evolution in the full nuclide and elemental breakdown of the material composition. These aspects are particularly important to nuclear materials modelling and design efforts, where the behaviour changes of both functional and structural materials under irradiation must be understood in detail. However, it is possible to provide even more information to materials damage modelling, and use the FISPACT-II system to evaluate primary damage response functions.

A new sub-program within the FISPACT-II system, called `SPECTRA-PKA` [28], has recently been prototyped and devel-

oped. By folding reprocessed (through the `groupr` routine of NJOY [29]) nuclear data in the form of recoil cross section matrices (see section 3.7) with an incident particle spectrum, `SPECTRA-PKA` will, for any nuclide composition, calculate the primary damage response in the form of primary knock-on atom (PKA) spectra for each nuclear reaction channel. It also outputs summed distributions as a function of recoiling species (heavy isotope, secondary-emitted gas particle, or element). Such distributions can be used as input to atomistic simulations – e.g. as sampling distributions to define the rate and energy of damage cascade events. Full details of the methodology in `SPECTRA-PKA` is given in [28, 30].

Figure 5 shows the results obtained from `SPECTRA-PKA` when a typical PWR neutron spectrum is folded with the neutron-induced recoil cross section matrices for TENDL-2015 for the nuclides present in a typical "as manufactured" composition of Inconel-718 (17.7 atm.%Fe, 19.0% Cr, 52.5% Ni, 3.0% M0, 5.1% Nb, 1.0% Ti, and other minor impurities including Mn, Si, Al, Cu). The plot shows the elemental results – i.e. where the recoils of different isotopes of the same element have been summed together into one PKA distribution. The figure demonstrates that it is not merely the input elements (highlighted in the figure legend) that make up the recoiling species under neutron bombardment, but rather that these are supplemented by PKAs of elements produced via direct transmutation nuclear reactions. This is confirmed by the even more complex picture at the isotope level, shown in figure 6, where the recoils of isotopes present in the starting material (again highlighted in red in the figure legend) only comprise around half of the total number of recoiling nuclides. Even more startling is that this is the zero-time picture, i.e. before the composition has been altered by nuclear transmutations. Within the FISPACT-II system it is readily possible to explore the change in the picture shown in figures 5 and 6 after a period of irradiation, by simply feeding the evolved nuclide composition into `SPECTRA-PKA`. Such an exercise in this Inconel-in-PWR case would result in the number of PKA species expanding with time, as nuclides are produced by transmutation and decay, thereby becoming targets for further damage events as the irradiation continues.

Note that in figures 5 and 6, it is nonetheless the case that the major constituents of Inconel-718, either by element (Ni, Fe, Cr) or isotope (^{58}Ni, ^{60}Ni, ^{56}Fe, etc.), do contribute the majority of the highest PKA rates at all recoil energies. This is due to the dominance (high cross sections) of the simple elastic and inelastic scattering reactions, which do not alter the impacted nuclide. The figures also show the potential importance of the recoiling secondary emitted (gas) particles, particularly protons and α-particles. The light species typically recoil with much higher energies that the main heavy recoil produced via, for example (n, p) and (n, α) reactions, and, despite their low mass, should therefore by considered carefully in damage creation modelling.

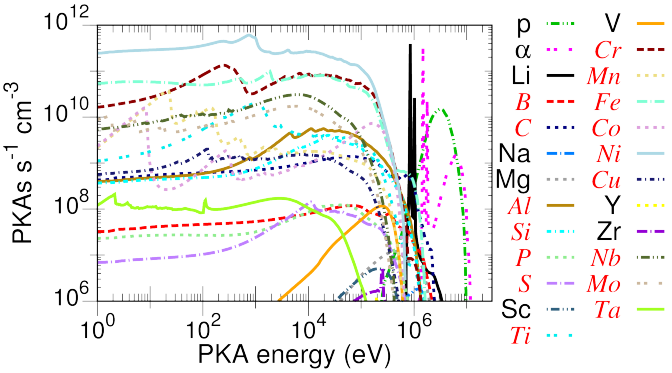

Figure 5: (Colour online) The primary damage state of Inconel-718 exposed to the typical neutron spectrum experienced in a PWR reactor. The curves represent the zero-time rates of primary knock-on atoms (PKAs) as a function of energy – summed by element – that would be produced in the material the instant the neutron exposure began. Elements already present in the Inconel are highlighted in italic red in the legend.

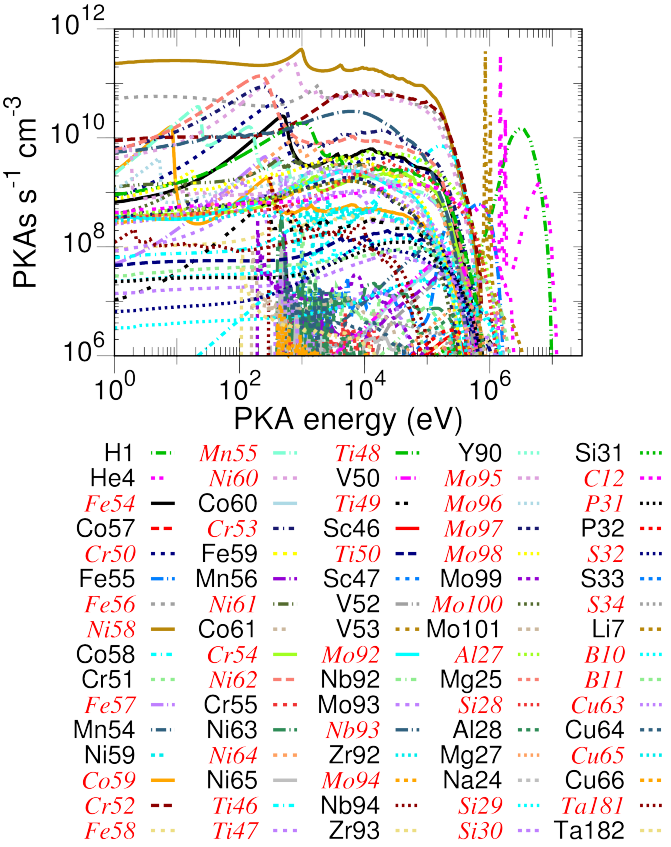

Figure 6: (Colour online) The primary damage state of Inconel-718 exposed to the typical neutron spectrum experienced in a PWR reactor. The curves represent the zero-time rates of PKAs as a function of energy – summed by isotope – that would be produced in the material the instant the neutron exposure began. Isotopes present in the Inconel before exposure are highlighted in italic red in the legend.

3. Nuclear Data Libraries

The new code system has benefited from the maturation of modern nuclear data libraries, now expected to include a full set of variance-covariance information and the amalgamation of the capabilities of the most recent release of three processing codes PREPRO, NJOY and CALENDF. Although the nuclear data forms available to the FISPACT-II inventory code are complete and complex in nature they mainly rely on an ENDF-6 format frame structure and this tremendously simplifies all further utilitarian operations such as plotting, comparison, concatenation and data manipulation in general. The nuclear data forms encompass group cross-sections (fine 660 group structure below 30 MeV and a 1102 extension of the CASMO-586 group), resonance parameters with covariance, probability tables, recoil daughter and emitted particle spectra matrices, spontaneous and particle-induced fission yields, and decay data, as well as biological, clearance and transport indices. The major libraries drawn upon for the FISPACT-II system are:

- **ENDF/B-VII.1** [31] American general-purpose library containing nFY and decay files
- **JENDL-4.0u** [32] Japanese general-purpose library containing nFY and decay files
- **JEFF-3.2/3.1.1** [33] European general-purpose library containing nFY and decay files
- **TENDL-2015** [22, 34] General-purpose libraries for 5 incident particles and all targets with $t_{1/2}$>1s. Produced with the T6, TALYS-based code package [35].
- **GEFY-5.2**[36, 37] Centre d'études nucléaires de Bordeaux Gradignan GEF-based fission-fragment yield library, where each file includes data for 59 incident energies from 0.0253 eV to 30 MeV.
- **UKDD-16** UKAEA decay data file built from EAF-2007 decay data [38] with inclusion of some updates and an increased set of short-lived nuclides to cover further TENDL radioactive targets and daughter nuclides

These data libraries vary in content, with the majority containing only a subset of the possible reaction channels, variance-covariance data, emitted particle double differential, etc. While there are many metrics to compare these libraries, various tables in the following sections summarise the number of incident-neutron, decay and fission yield files from the major libraries.

3.1. Cross section group structure

There are three standard group structures in the ENDF-6 format used for the TENDL, ENDF/B.VII.1, JENDL-4.0, CENDL-3.1 and JEFF-3.2 nuclear libraries. Data in these structures can be read automatically into FISPACT-II and used to collapse with an incident particle spectrum in the corresponding structure.

Each possesses a fine energy grid, an increased upper energy bound of 1 GeV, and allow the addition of α and γ-induced reactions while permitting more precise modelling of reaction thresholds and the resolved and unresolved resonance ranges. These groups are the CCFE-162 (charged particles), CCFE 709 (TART-660 extension) and the UKAEA-1102 (an amalgamation of CASMO, TART and UKAEA fast group structures).

The group structures for the UKAEA-1102 and its predecessors are shown in Fig. 7, depicted in equal energy bin width, lethargy and cumulative number of energy groups. These illustrate which energy ranges are targeted by each structure and will therefore give an accurate representation of the reaction rates.

The CCFE-162 (up to 200 MeV) structure was introduced for studies of charged-particle projectiles and γ-induced activation and transmutation. This structure includes all legacy ones known to the author, because past limitations of computing resources are no longer a consideration justifying simpler energy structures. The CCFE (709 up to 200 MeV and 660 up to 30 MeV) group structures are extensions of the LLNL (616 up to 20 MeV) structure. They have 50 tally bins per energy decade, equally spaced in the logarithm of the energy between 10^{-5} eV and 10 MeV, 200 keV steps to 30 MeV and thereafter bins with appropriately chosen equally-spaced boundaries in energy up to 1 GeV. The UKAEA 1102-group structure is the culmination of extensions of the state of the art thermal fission CASMO (586), the fast LLNL (616) and the fast CCFE (709) structures pushed to 1 GeV. Each specific feature of those three grids have been combined into one single structure: the UKAEA 1102-group structure depicted in Fig. 8.

The generation of reaction rates with multi-group convolution of binned fluxes with cross-sections has always been the subject of intense research in order to satisfy the specific requirements of one application at a time. Recent studies [39, 40] have demonstrated that the fine CCFE-709 and *a fortiori* the UKAEA-1102 group structure have been optimised to comprehensively cover most applications.

3.2. Particle-induced reaction data

FISPACT-II accommodates a range of nuclear reaction data forms, including induced-reaction cross sections for multiple incident particles, for example, but not limited to TENDL-2015, ENDF/B-VII.1, JEFF-3.2, JENDL-4.0u and CENDL-3.1 nuclear data libraries processed into a fine-group structure. The recommended cross section data libraries for FISPACT-II are the TENDL ENDF-style forms, mainly because they have the ability to provide the most complete datasets and forms including variance and covariance information. Those libraries have been the subject of a wide range of verification and validation processes.

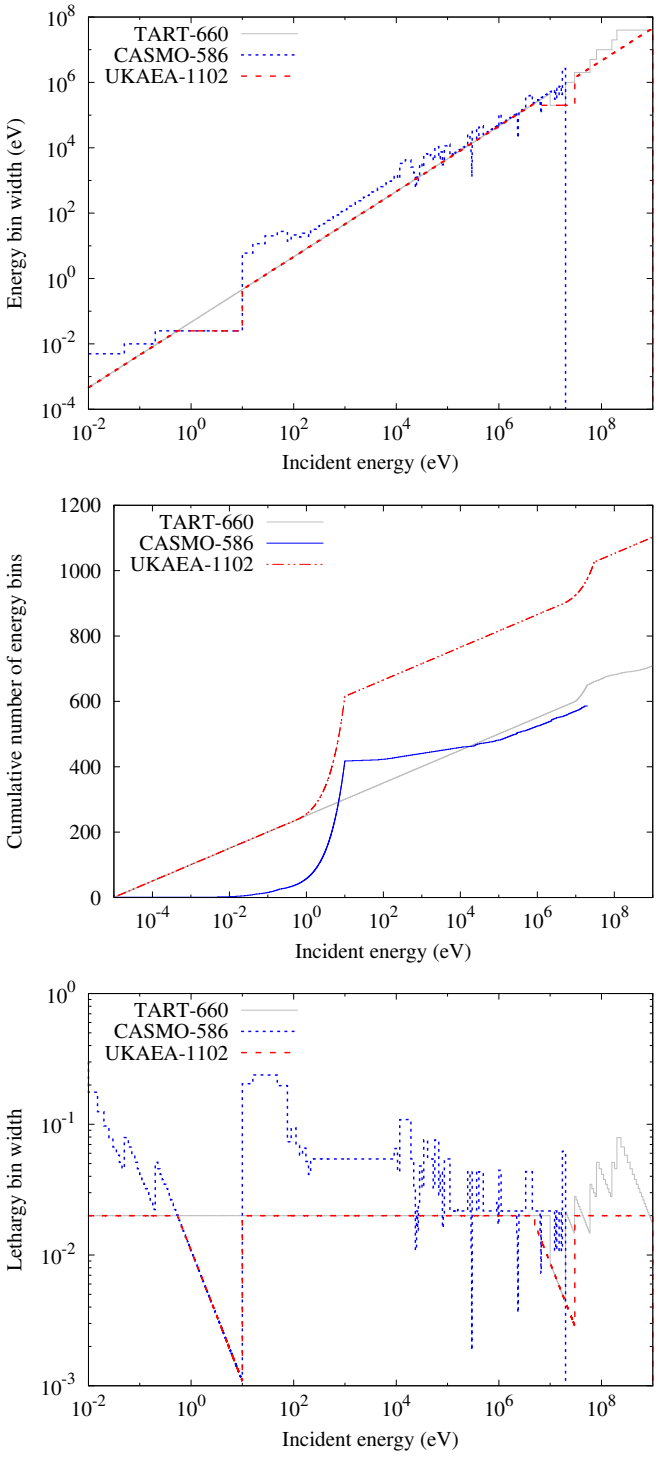

Figure 7: (Colour online) Energy group structure for the TART-660, CASMO-586 and UKAEA-1102 group structures. Three plots, from top to bottom, show the (1) energy bin width, (2) cumulative number of energy groups and (3) lethargy bin width as a function of incident particle energy.

The enhanced cross section and data forms for FISPACT-II are entirely ENDF-6 compliant in nature and are more robust, complete and more exploitable with regard to any application than the raw data they are derived from. The `MF` (files) and `MT` (channels) legacy ENDF-6 infrastructure dictionary is kept and processed, but also complemented when needed. Derived, reconstructed `MT`s are added: such as partial gas production, total and partial kerma and dpa, complete isomeric channel partial cross sections properly parsed and stored in `MF`=10, as are the light particle (A<4) and heavier radionuclide production cross sections at high energy, above 30 MeV, in a comprehensive `MF`=10, `MT`=5 description that details the production cross sections for up to 200 daughter radionuclides.

Cross-section and probability tables are given for three reactor temperatures in the Kelvin range. Two astrophysics temperatures in the keV range are also given for the major libraries.

It should be noted that the full `MF`=2, `MT`=152 data are kept in their original state in the processed file to be used when requested by FISPACT-II's self-shielding keyword. PKA matrices for the heavy recoils and the light particles are also given for all the stable nuclei in the same 660 up to 30 MeV group structures.

Variance and covariance data are also processed directly with FISPACT-II but then only if they exist in part or in full in the original evaluation and library. Only TENDL systematically and uniformly contains such information. All the libraries are for neutron-induced reactions, but TENDL also provides α, γ, proton and deuteron-induced datasets, ENDF/B-VII.1 provides γ-induced reactions and JENDL-4 also provides a set of high-energy proton, neutron and a few α-induced evaluations.

Each library has its own tree-based directory structure that contains files for single nuclides, named after the isotope they refer to. Such simple storage infrastructure gives robustness, efficiency and flexibility.

3.3. Processing methods

The NJOY processing system is widely used to convert evaluated files into forms of interest for numerous practical applications. Many reactor analysis, criticality safety, radiation shielding, inventory simulation codes rely on its powerful processing capabilities to provide their (often specialised) nuclear data forms. Uniquely, in addition to the processing of cross sections, angular distributions, emitted spectra and other nuclear observables, NJOY can be used to process:

- gas production reactions: `gaspr`;
- heat production cross sections: `heatr`;
- displacement cross sections: `heatr`;
- charged particle and recoil energy group-to-group matrices: `groupr` (see section 3.7).

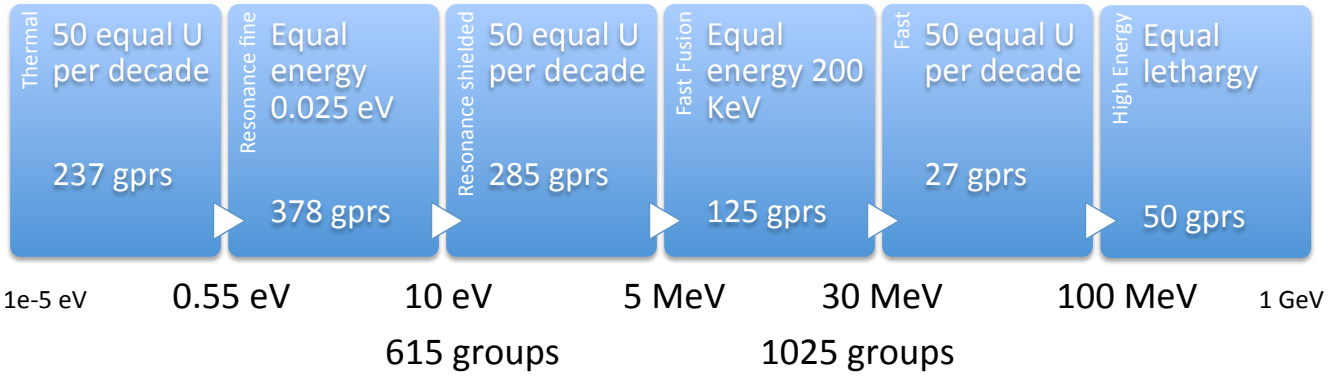

Figure 8: (Colour online) UKAEA-1102 group structure description.

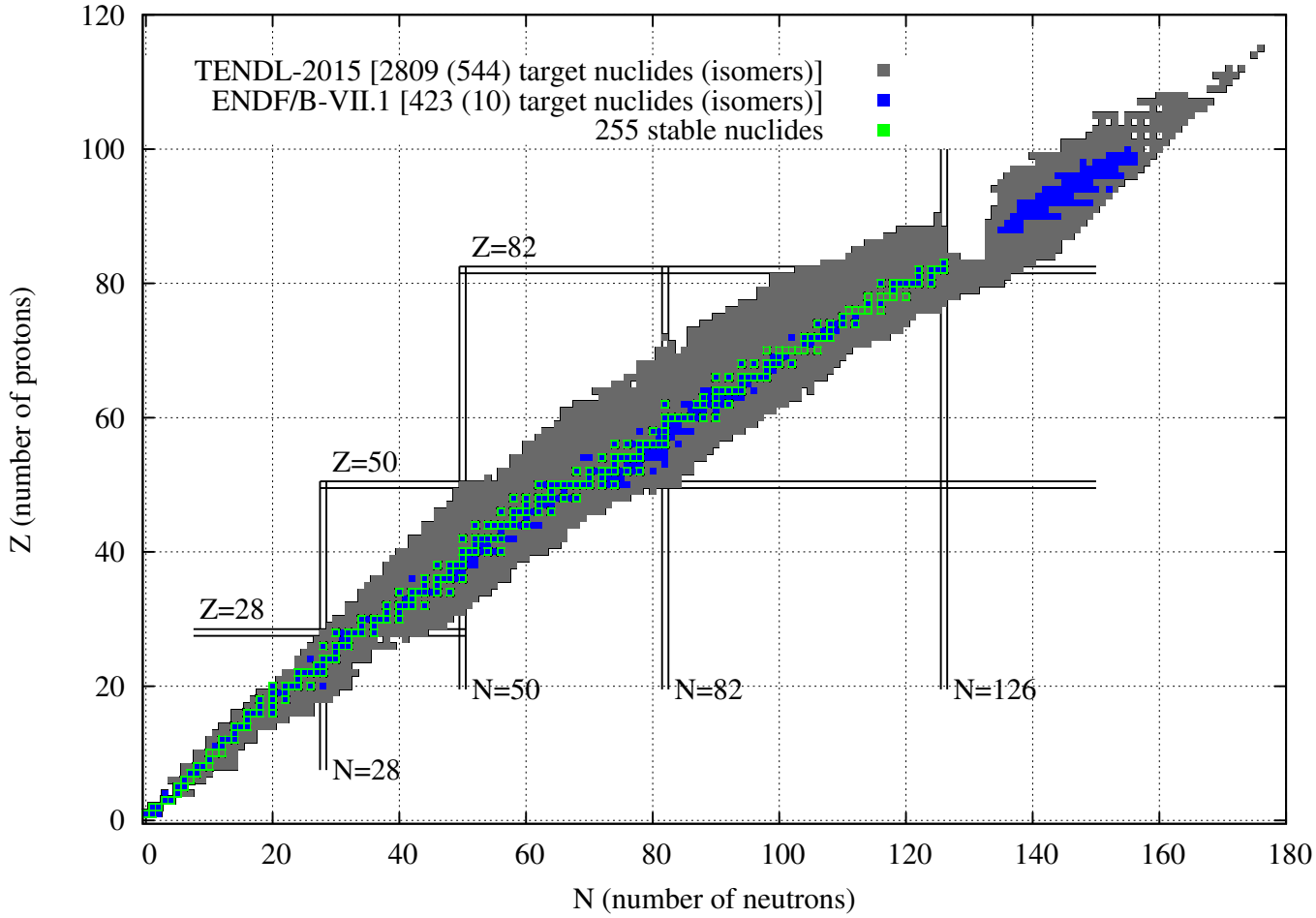

Figure 9: (Colour online) Chart of nuclides showing the range of all TENDL-2015 target files against the same for ENDF/B-VII.1.

Table 5: Summary of nuclear data forms supplied in the standard FISPACT-II distribution.

Library name	Number of target nuclides	Variance and covariance	Number of nuclides with probability tables	Temperatures	PKA matrices
TENDL-2015	2809	All	2601	293.6 K 600 K 900 K 5 keV 30 keV	Yes
ENDF/B-VII.1	423	190	268	293.6 K 600 K	Yes
JENDL-4.0u	406	Few	292	293.6 K 600 K	Yes
JEFF-3.2	472	Few	0	293.6 K 600 K	No
CENDL-3.1	239	Few	0	293.6 K	No

Application forms for FISPACT-II include all the above. The first three, once generated in the specific NJOY pointwise format are extracted and seamlessly embedded into the PREPRO pointwise infrastructure for proper integration and further processing.

The charged "light" particle (A≤4) and "heavy" residual nucleus (A>4) recoil group-to-group matrices are also produced from the `groupr` module of NJOY in the same fine group structure as for the cross section for each evaluation. Those can then be folded, isotope by isotope, with any neutron spectrum to provide materials science applications with the recoil energies information they need at an elemental level. However, this type of practical information form is satisfactory only if the original evaluation is complete and fully populated. Older evaluations produced specifically for fission reactor physics applications may be inadequate in this respect.

NJOY can also be used to process some parts of the variance and covariance information, however in the case of FISPACT-II requirements it has been necessary to consider a specific development in order to be able to master the full complexity of the data streams necessary to an inventory code. As described in Section 2.1.1 a projection operator maps the cross-section energy bins to the covariance energy bins.

The PREPROcessing codes are designed to pre-process ENDF-6 formatted data into forms useful for applications. PREPRO is a modular set currently comprising 18 modules each designed to perform one or more independent operations, that are used in a given sequence. Raw ENDF-6 data files need to have resonance parameters interpreted for cross sections to be constructed, Doppler broadened, thinned and linearised to the desired temperature, with isomeric branching ratio applied when necessary, before being in a form usable for applications.

The recent release of PREPRO-2015 consists of an important modernisation of all codes, following the latest requirements linked to the ENDF-6 format, specifically: portability, level of precision and latest Fortran. It also comes with a set of "best input parameters" that allows safe but robust data mining and processing activities.

Application forms of use for FISPACT-II generated from PREPRO (using the `linear`, `recent`, `sigma1`, `sixpack`, `activate`, `merger`, `dictin` and `groupie` modules) include detailed partials, total group cross sections, resonance widths and uniquely high energy (>30 MeV) activation and transmutation cross sections, and radionuclide yields (when provided in the original data set). PREPRO also merges the unique NJOY-produced set of responses, kerma, displacement cross sections and gas production, into its own structures. Finally, one of its modules groups all cross sections into a fine structure using appropriate micro flux weighting spectra.

One tremendous advantage to be gained from this particular suite of modules and processing steps is that at any stage it endeavours to keep the output file structure in ENDF-6 format, file and reaction-type numbers alike. Cross sections constructed from parameters progress from 0 K pointwise data, to 293.6 K pointwise then groupwise data in the same structured file.

3.4. Decay data

In addition to cross sections the other basic quantities required by an inventory code are data on the decay properties (such as half-life, α, β, γ emissions, etc.) of all the nuclides considered as targets or daughters. These data are available in the various evaluated decay data libraries. FISPACT-II is able to read the data directly in ENDF-6 format; it requires no pre-processing to be done, although file debugging has always been found necessary. Earlier libraries were based primarily on the JEFF-3.1.1 [41] and JEFF-2.2 [42] radioactive decay data libraries, with additional data from the most recent UK evaluations. However, not all of the then 2233 nuclides that were needed at the time are included in such sources. For these nuclides data were taken from sources such as Brown and Firestone [43], and ENDF-6 formatted files have been constructed. Reference [44] documents the earlier library, but in order to handle the extension in incident particle type, energy range and number of targets, many more nuclides are needed. A new 3875-nuclide decay library named UKDD-12 has been assembled from previous compilations, complemented with all of JEFF-3.1.1, a few nuclides from ENDF/B-VII.1 and other decay files to cover the range of daughters arising from all TENDL reactions and more short-lived fission products.

Care has been taken to ensure that the cross-section and decay data libraries are compatible. All nuclides (in-

Table 6: Decay libraries.

Library name	Number of isotopes
UKDD-12	3875
JEFF-3.1.1	3854
ENDF/B-VII.1	3818
JENDL-4.0	1380
JDDF-2015	3237

Table 7: Fission libraries.

Library name	nFY	sFY	oFY
GEFY-5.2	119	109	
UKFY-4.1			21
JEFF-3.1.1	19	3	
ENDF/B-VII.1	31	9	
JENDL-4.0	31	9	

cluding isomeric states) that can be formed from the various reactions as daughters in the cross-section library need to be included in the decay library so long as their half-lives are greater than 0.1 second. Some nuclides with shorter half-lives are also included where it is felt that they are of particular importance (e.g. the metastable states of ^{88}Y). Short-lived (<0.1 s) isomers which would return to the ground state by an isomeric transition usually have little impact on activation calculations and most of these have been ignored so far. However, the effort is now directed towards better physics and completeness, rather than accepting pragmatic solutions.

There are still some issues regarding minor differences between the isomer definitions in the cross-section library (arising from the RIPL-3 database used in the preparation of TENDL) and those in the newly-compiled decay library. FISPACT-II now handles ground states and several isomeric states (g, m, n, o, ..., t) but there are some inconsistencies in the energy levels of these radionuclide daughter products of reactions and the associated decay data files. These inconsistencies will be addressed fully in a future release of the system.

3.5. Fission yields

The FISPACT-II inventory code allows the use of a variety of neutron-induced (nFY), spontaneous (sFY) and particle-induced (oFY) fission libraries. Cumulative or independent yields can be selected. The various libraries contain not only different data for the same nuclides, but also cover different sets of nuclides. This is summarised in Table 7, which shows the number of nuclides with data for neutron-induced fission yield, spontaneous fission yield and alpha, deuteron, proton and gamma fission yield files. The methodologies behind TENDL and GEF [45, 36] allow for more robust files, notably containing any target nuclides, including isomers and a large range of incident neutron energies.

Fission yields are generally stored for three separate incident neutron energies: a thermal value of 25 meV, a fast value of 400 keV and a high-energy value of 14 MeV.

The GEFY-5.2 [37] data sets cover independent and cumulative fission-fragment yields where multi-chance fission is considered, fundamentally modifying the mass and general nuclide yields. The yields cover from thermal energy (0.0253 eV) to 30 MeV in 59 energy steps for all target isotopes, allowing a more sophisticated interpolation of the yields depending on the incident particle spectrum. Examples of the energy-dependent yields are shown in Fig. 10.

3.6. CALENDF probability tables

CALENDF is an R-matrix analysis, processing code with unique capabilities that complement the other processing codes. It has been widely used in the multi-physics data processing of the libraries needed by the FISPACT-II code. In the preparation of TENDL, CALENDF has been used both to generate statistical resonances for those target nuclides with no, or only poor, experimental information (Fig. 20), and also to extract and assemble the probability tables from all evaluations of resolved and statistical resonance parameters.

Probability table data sets are supplied for each evaluation/library and temperature from the energy of 0.1 eV up to the end of the unresolved energy range of the evaluation in the same fine group structure as the cross sections; 709 or 1102 groups. Several groups are typically not populated as they are outside the resonance energy range of interest. The same probability table forms are used by the Monte Carlo code TRIPOLI [46, 47] in the unresolved energy range and by the fast deterministic code ERANOS [48, 49] in both resolved and unresolved resonance energy range.

The code manipulates these probability tables in various ways, including isotopic smearing, condensation, interpolation and order reduction. Effective cross sections and moments can then be extracted in the resolved and unresolved resonance ranges, while probability table self-shielding factors (ssf) are calculated (Fig. 3) for any competing channels and isotopic compositions . Note that the effective cross sections and moments derived in this way account not only for contributions to the self-shielding factors from all known channels and energies but also any isotopic mixture. There is some overlap of probability table capabilities with PREPRO and NJOY, but the different codes are used as appropriate for the different forms [14] of application data.

3.7. PKA matrices

The group-to-group recoil cross section matrices required by the primary damage evaluation code `SPECTRA-PKA` (section 2.5) are produced by feeding the raw point-wise

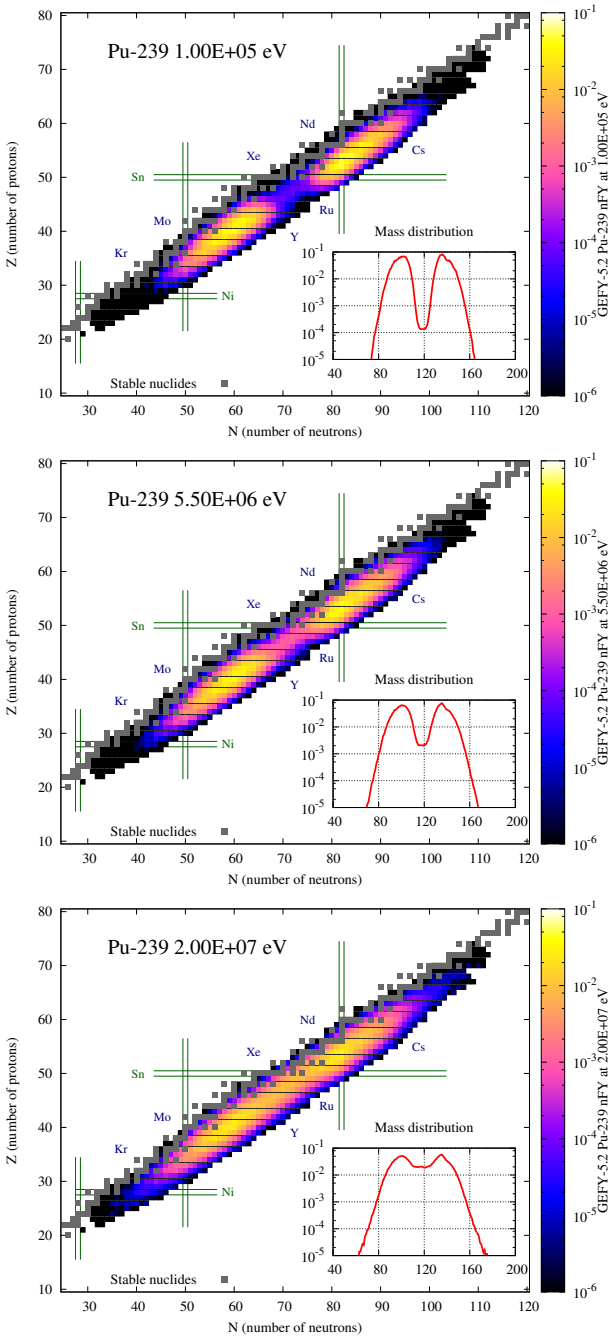

Figure 10: (Colour online) Energy-dependent neutron-induced fission yields from GEFY-5.2, showing the range of distributions. Incident energies shown include 100 keV, 5.5 MeV and 20 MeV.

evaluations of TENDL (and other libraries) into NJOY and outputting via a specially-modified for the purpose version of the `groupr` subroutine (the minor changes therein simply redirect the usual group-to-group matrix output to separate file streams, and use extra floating precision). A plottable version of the file for each target nuclide is also output.

Figure 11 shows a typical matrix, in this case for the pure elastic scattering channel on ^{184}W in TENDL-2015. The cross sections, as a function of recoil energy, are plotted for several incident energy groups (only a small subset of the 709 groups used to represent the TENDL-2015 data) – in essence each curve represents a different incident-energy column of the recoil cross section matrix for this reaction channel. As would be expected for elastic scattering, the cross sections are highest at lower incident energies, but produce less-energetic recoils.

Figure 12 shows another example, in this case for the (n, α) reaction on the same ^{184}W nuclide. This time there are two distributions: one for the heavy ^{181}Hf recoil (in grey); and another for the emitted light α particle (in blue). For this threshold reaction there are no significant cross sections below around 10 MeV. As would be expected, the recoil energies of the α-particle are significantly above those of the heavy residual. However, note also in this case, that the reaction has a positive Q-value of 7.3 MeV, which means that the energy of the α-particle can actually be higher than the incident neutron energy. In the figure this point is exemplified by seeing that the cross section curves associated with the α-particle of (n, α) are above in recoil energy to the incident=recoil energy line (red line in plot).

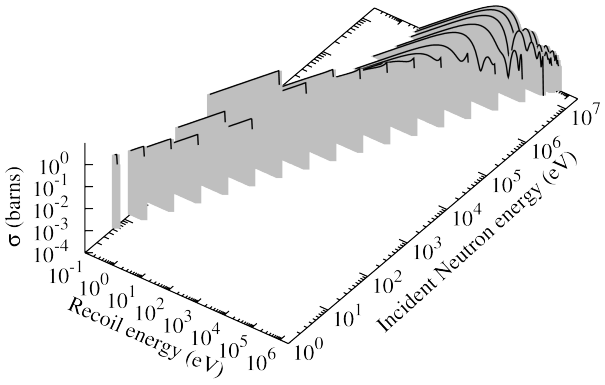

Figure 11: (Colour online) Representation of the group-to-group recoil cross section matrix for elastic scattering on ^{184}W - TENDL-2015.

4. Verification and Validation

Verification and Validation (V&V) activities are essential for the successful development of any well-engineered physics prediction code. An essential activity is verification to ensure that at all stages of the development the

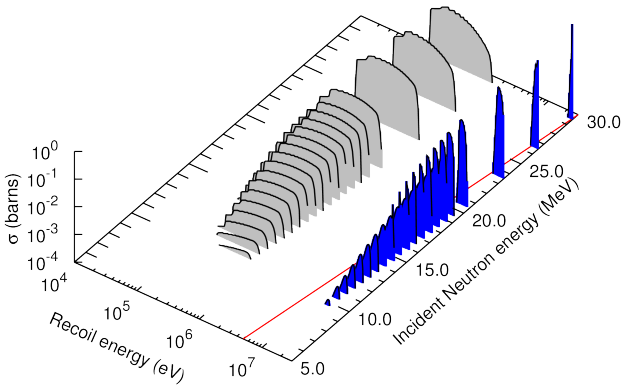

Figure 12: (Colour online) Representation of the group-to-group recoil cross section matrix for the ^{184}W$(n,\alpha)^{181}$Hf reaction - TENDL-2015. The cross sections for ^{181}Hf are shown in grey, while the higher energy α recoil cross sections are in blue. The red line in the base xy-plane represents incident=recoil energy.

code functions in accordance with its user requirements. Successful verification should then be followed by validation involving the comparison of results with external sources of information to ensure that the code produces correct results, or at least results of acceptable accuracy, taking into account the level of physics assumptions and approximations inherent in the design of the code and its input data.

The development of FISPACT-II has proceeded over several stages in recent years, with new features being added at each stage. An extensive set of test cases (currently several hundred) has been produced and extended as the code development has continued. This test set exercises all keywords that users employ in the FISPACT-II `input` file to control a run of the code. The test cases ensure that newly-added keywords have the intended effects. The test set also provides regression tests so that all the established functionality of the code can be verified each time a new release is prepared.

Verification and validation is a vital part of the processing and production of nuclear data libraries. For an advanced inventory and observables code which covers the complete set of nuclear reactions, this takes several forms:

- validation of input nuclear data against experimental information, both integral and differential;
- verification of the nuclear data, particularly those without experimental information, against systematics, statistical review and consistency checks;
- checking code methodologies for nuclear data interpretation, reading, processing and use in simulations – essential for handling multiple ENDF-6 libraries and technological databases such as TENDL and GEFY;
- validation of code simulations against experiment for all input nuclear data forms.

In the last few years great effort has been expended on producing a set of, largely-automated, V&V tools. As well as validating the nuclear data libraries themselves, these V&V tools also verify the robustness and accuracy of the FISPACT-II code itself. Each individual report straddles multiple aspects of the general V&V process, for example the integro-differential report tests TENDL effective cross sections against experimental data as well as differential EXFOR and full code simulations against a variety of integral measurements. Each section discusses one aspect of the V&V with a brief summary of salient conclusions from one of the reports.

4.1. Fusion decay heat

Little experimental data exists for structural material samples irradiated under all nuclear plants relevant neutron spectra and even when data does exist the measured quantities are either specific activity and/or γ spectroscopy. In particular, no or very little experimental data on decay power has previously existed for fission plant structural materials and for materials under high energy irradiation conditions (i.e. fusion, fast fission). It was to fill this gap that a series of experiments were performed using the Fusion Neutron Source (FNS) facility at the Japan Atomic Energy Agency JAEA [50, 51, 52] . Material samples were irradiated in a simulated D-T neutron field and the resulting decay power was measured for cooling times of up to thirteen months. Using the highly sensitive Whole Energy Absorption Spectrometer (WEAS) method, both β and γ emission decay energies were measured at selected cooling times and, quite impressively, as soon as a few tens of seconds after the end of irradiation.

Validation of decay power predictions by means of direct comparison with integral data measurements of sample structural materials under neutron spectra allow confidence to be given to the decay power values calculated. It also permits an assessment of the adequacy of the methods and nuclear data, and indicates any inaccuracy or omission that may have led to erroneous code predictions. It is clear that certain safety margins can be derived from such a validation exercise, if relevant to plant operation, materials and design, and applied as bounding conditions in operational Safety and Environmental (S&E) analyses.

4.1.1. FNS Assembly

14 MeV neutrons are generated by a 2 mA deuteron beam impinging on a stationary tritium-bearing titanium target. The total neutron flux at the sample location, for this experiment, is in the range of 1.0×10^{10} [n cm^{-2} s^{-1}], the same order of magnitude as in the first wall of the Joint European Torus (JET) fusion experiment when operating with D-T plasma. However, the irradiation time at the FNS were of 5 minutes and 7 hours in comparison with the few seconds flat burn achieved during the DTE1 JET fusion 1996 campaign. As a point of reference the total flux in a power plant is typically expected to be in the

region of 10^{13} or 10^{15} [n cm^{-2} s^{-1}], three to five orders of magnitude higher than in JET or FNS, and also for much longer irradiation times.

Thin samples, 25x25 mm^2 in area, and typically 10 μm thick, have been used, either as metallic foil or powder sandwiched between tape. Use of a thin sample minimises the self-absorption of β rays emitted in the sample itself and allows their measurement. A total of 74 different materials have been used across the different phases of the experiment.

The decay energy in each irradiated sample was measured in the Whole Energy Absorption Spectrometer (WEAS), which comprises two large bismuth-germanate BGO scintillators in a geometric arrangement, provides almost 100 % detection efficiency for both β and γ-rays. Correction factors need to be applied for γ-ray efficiency and for β and electron energy loss in the sample itself (less than 15% generally), and for other effects such as the decay heat due to the plastic tape used for the powder samples. The overall experimental uncertainty totals between 6 to 10% in most cases, although it rises to higher levels at particular cooling time for certain samples. The WEAS provides high sensitivity, down to powers less than 1 pW, which is valuable for measurement of some nuclides with long half-lives. It also has a wide dynamic range: measurements of up to a few mW have been achieved in the experiments.

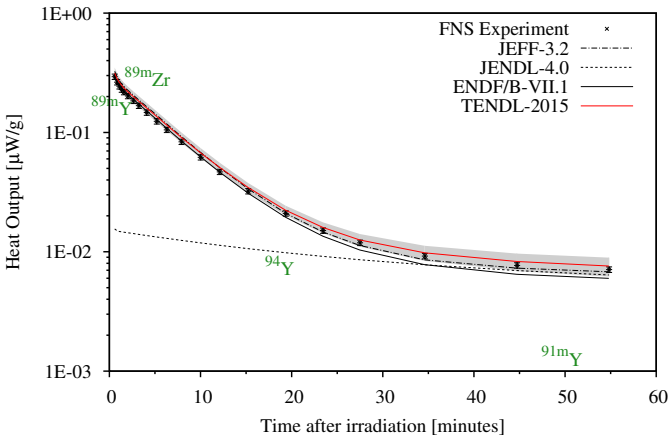

Figure 13: (Colour online) Decay heat production and cooling in zirconium irradiated for five minutes in the JAEA FNS experiment, compared with FISPACT-II predictions. TENDL uncertainty as shaded area.

4.1.2. Comparison of the Results

For each material sample and irradiation condition, FISPACT-II, combined with the TENDL-2015, ENDF/B-VII.1, JEFF-3.2 and JENDL-4.0, calculations have been performed [53, 54]. Graphical comparisons of the results are presented. On the graphs FNS experimental measurements are also plotted and include the uncertainties as vertical lines, while the grey shadow area corresponds to the

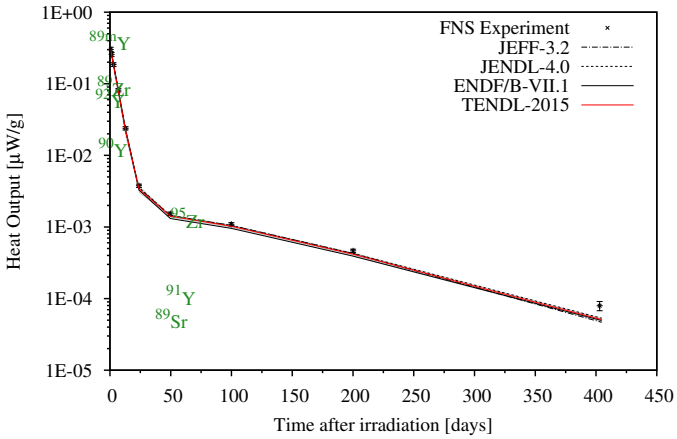

Figure 14: (Colour online) Decay heat production and cooling in zirconium irradiated for seven hours in the JAEA FNS experiment, compared with FISPACT-II predictions.

calculation uncertainty derived from TENDL-2015. The 5 minutes or 7 hours irradiation results can be presented. Care needs to be taken when interpreting the graphs, particularly in view of the log-linear scales. Such plots allow a direct visual interpretation of nuclide half-life at times when one isotope is clearly dominant. A departure from equivalence in the decay profile between experiment and calculation would indicate a mismatch in terms of half-life in one or more of the important nuclide.

The full report details the analyses for each of the 74 materials samples that have been irradiated in the two campaigns. To complement the analysis of total heat, an appendix has been included showing the TENDL-2014 differential cross sections against EXFOR [55] for all reactions leading to the production of dominant nuclides. Further details of these plots can be found in [56].

There is some interest in focusing on irradiated sample of importance for one applications. Zirconium is largely employed as cladding material in many LWR plant worldwide and as such deserve some attention. From Fig. 13 one immediately notice a good agreement amongst the different nuclear databases but for JENDL-4.0 unable to produce ^{89m}Zr, predominant in the first half hour of cooling. Time dependent calculation over experiment (C/E) values (2-18%) also compare nicely with the TENDL-2015 derived uncertainty (8-20%). From the longer irradiation, longer cooling time graphs shows in Fig. 14 one may deduced much better overall performance. Note that the decay heat dropped by three orders of magnitude within a month cooling.

Nickel and niobium, Fig. 15 and 16 are also elements of importance in the next generation of power plants, fusion or fast fission, however in those particular cases one has to remarks the lack of isomeric production channels from the legacy libraries. Only the truly general purpose TENDL

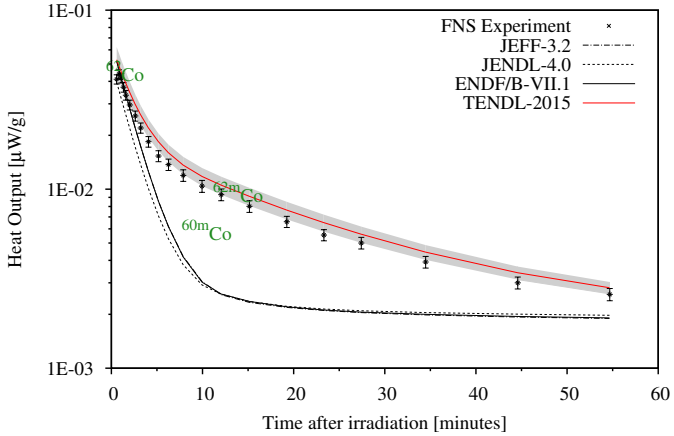

Figure 15: (Colour online) Decay heat production and cooling in nickel irradiated for five minutes in the JAEA FNS experiment, compared with FISPACT-II predictions.

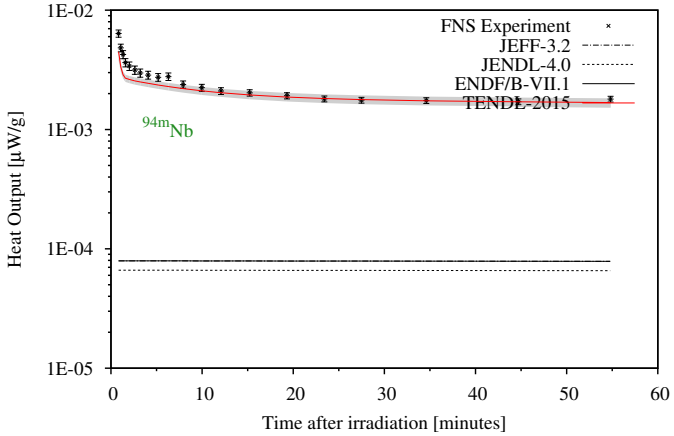

Figure 16: (Colour online) Decay heat production and cooling in niobium irradiated for five minutes in the JAEA FNS experiment, compared with FISPACT-II predictions.

library seems to be capable of reproducing the more exact time dependent decay heat profile arising after irradiation of those elements. What is also of concern is the systematic under prediction, by lack of isomeric state branching ratio, from the other libraries. Having said that Fig. 17 demonstrates the opposite, for an important neutron absorbent material: silver.

4.1.3. FNS Analyses

The experimental time-dependent decay-power measurement program at JAEA FNS combined with the FISPACT-II simulations performed provide a unique check of the calculational method and nuclear databases associated with the prediction of decay power for the set of material samples analysed. The results of the comparison give confidence in most of the decay heat values calculated, although the predominantly 14 MeV neutron spectrum in FNS means that the low neutron energy reactions of importance in other devices have not yet been fully considered [57]. This statement limits the scope of validation and possible conclusions reached in this study to the decay power predicted through the identified pathways. However, it covers the decay data of all the isotopes involved irrespective of their production routes.

The experimental uncertainty, calculational uncertainty and E/C values have been systematically produced. Their direct comparison demonstrates that the method chosen to calculate and propagate these calculational uncertainties in the FISPACT-II code system is verified and validated (V&V), and that the TENDL uncertainties file could be further improved along the same lines.

From the overall results, a set of inadequacies, not only in the cross sections but also in the decay libraries, have been identified that will require some corrective actions to be taken. These corrections and/or amendments will benefit the next generation of the TENDL library cross sections, associated variance and covariances, and decays data files. As expected, they impact both the production paths and/or decay data of some specific radionuclides without impairing the overall picture. A large proportion of the decay powers calculated in this validation exercise with TENDL-2015 are in good agreement (within a few %) with the experimental values for cooling times spanning from tens of seconds, and this is a unique insight in the isomers space, up to more than a year.

4.2. Integro-differential

For a great many target nuclides and reactions, there are few experimental measurements to rely upon in the nuclear data evaluation process. Many energies are too difficult to probe, for example resonance regions or energies between a few MeV and 14 MeV for neutrons. These limitations in the data force us to be more proactive in validation, drawing upon different, complementary sources to draw conclusions where individual sets of differential measurements are lacking.

A series of irradiations of various materials in several complementary neutron fields have been carried out over several decades. Analyses of the results have produced integrated effective cross sections attributed to various nuclear interactions. Neutron spectra calculated for each experiment can be convolved over energy with library cross sections for comparison with experimental results. The measurement techniques vary between experiments, from calorimetric to spectroscopic, fairly mono-energetic to 'white' spectra. Each presents its own challenges, but the extraction of useful data on individual reaction channels can be done even in calorimetric measurements such as those performed with total decay heat from FNS.

To best gauge the quality and extent of the conclusions that can be drawn from the available set of integral

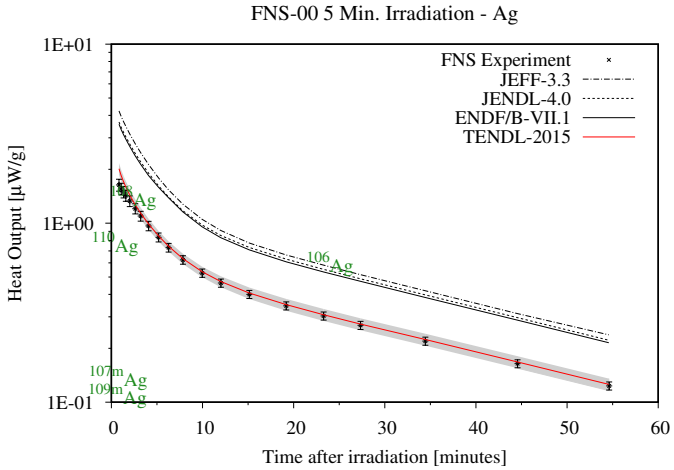

Figure 17: (Colour online) Decay heat production and cooling in silver irradiated for five minutes in the JAEA FNS experiment, compared with FISPACT-II predictions.

measurements, differential data from EXFOR is compared against the evaluated cross sections with all isomeric production, if present. The combination of these has great value in highlighting areas for re-evaluation or providing the most robust activation validation possible.

The combination of multiple, complementary integral measurements with differential cross-section data from EXFOR has been used to validate the TENDL-2014 neutron-induced nuclear data library. The integral measurements use incident particle spectra from a variety of sources including:

- Fusion D-T with various amounts of scattering, 14 MeV peaked
- Deuterium beam on beryllium target 'fast white' spectrum above 20 MeV
- Deuterium beam on lithium target 'IFMIF-like' spectrum up to 60+ MeV
- Proton beam on deuterium targets 'fast white' spectrum above 20 MeV
- Spontaneous ^{252}Cf fission neutrons

The measurement techniques typically include HPGe gamma spectroscopy to identify individual nuclides, spectroscopic or total heat measurements. Normalisations and spectra are determined through various means, from activation foils to ToF and alpha-monitors. Not all experiments are of the same quality and this fact is extremely important when making judgements on the quality of an evaluated file using few measurements.

Identification of individual reaction channels within integral measurements poses a few challenges, including the separation of production of decaying, precursor nuclides (cumulative effects) and isolation of multiple reaction channels, which occurs through multiple target elements, multiple target isotopes and multiple reaction channels per nuclide. Care must be taken not to mistakenly identify one reaction channel with multiple are involved, which could either throw into question an accurate evaluation or 'validate' a spurious cross section. The approach taken by the UKAEA is to establish a set of criteria for inclusion and remove those which fail the tests. In those (few) cases removed which were used in previous EAF validations it is unlikely that the experiments measured the specific reaction channel(s) in question.

For all integral measurements new pathways analysis using the FISPACT-II pathways search features have been done. These identify the % contribution from each reaction channel and verify that the channel of interest is dominant for the measurement. Even with high-purity samples this can be quite complex due to multiple isotopes or reactions, for example the FNG nickel irradiation shown in Fig. 18. As in several cases, the total heat measurements reflect multiple nuclides contributing at every time-step. However, at specific points one nuclide is strongly dominant, for example the ^{62}Co and ^{62m}Co at the first and last measurements shown in this figure. Decay data can provide an additional concern due to potential misallocation of beta/gamma heat (and other more simple issues such as half-life uncertainty). The apparent discrepancies between beta and gamma heat in the first measurement are reconciled in the total, which has a less uncertain energy per decay. ^{60m}Co dominates the gamma heat at 500 s and ^{62m}Co dominates the beta and total in the final point. The production pathways for nickel are quite simple, with ^{60}Ni(n,p) and ^{62}Ni(n,p) generating the cobalt isotopes and isomers. This allows specific identification of each as an integral measurement of a reaction channel.

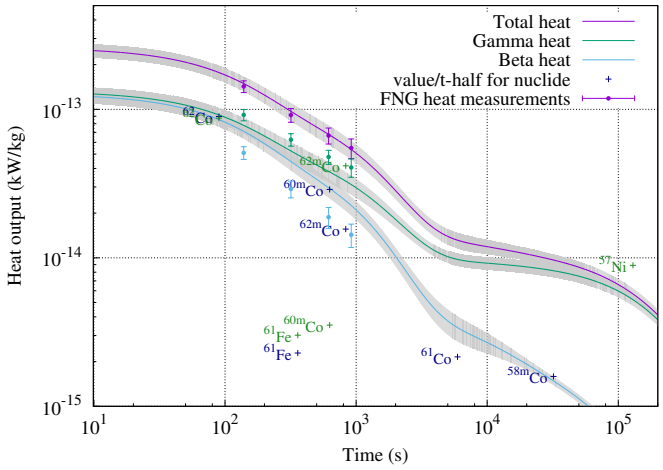

Figure 18: (Colour online) Total and spectroscopic decay heat measurements from an FNG irradiation of nickel with FISPACT-II predictions. Dominant nuclides are placed at coordinates which reflect their half-life and end-of-irradiation heat.

This level of analysis has been performed in the recent report for the FNS and FNG (Frascati) heat measurements. Results from other laboratories were tested with pathways analyses and verification of the reaction channels available.

Care must be taken when claiming that a reaction has been 'validated', since the detailed structure of a cross section is not fully probed (even with multiple experiments using complementary spectra) and a new experiment using a different spectrum could find discrepant results. Aside from the differences in experimental design, there is tremendous deviation in the quality of the spectral characterisations, simulation tools used to calculate data (ultimately including the effective cross section) and reporting of measurement methodologies.

The distributions show a generally superior agreement for TENDL-2014, with 12% more values between 0.94 and 1.06. The log-mean C/E value,

$$\log\left(\overline{C/E}\right) = \frac{1}{n}\sum_{i=1}^{n}\log\left(C_i/E_i\right) \ , \qquad (49)$$

for TENDL-2014 is 0.993, while the EAF-2010 data yields a surprising 0.850. This can be intuitively seen in the skewed EAF distribution of C/E values, indicating a systematic under-prediction for the integral values of this report. The fact that TENDL provides a more symmetric distribution should not be surprising; the data is derived from physical parameters which globally govern the production of reaction information and both under- and over-prediction should be equally likely. In comparison, the asymmetry of EAF belies its methodology, where pathways are included depending on an evaluator's judgement. As a result, pathways are missing or under-represented and result in an overall under-prediction for nuclide production.

It should be noted that the EAF library was constructed and modified with knowledge of these integral measurements, which were used as justification for renormalisations leading to better agreement with the experiments. That TENDL blindly predicts these effective cross sections, using physical parameters, with greater accuracy than a library tuned by renormalisations is quite remarkable. When the standard international libraries are used to calculate the effective cross sections considered the distribution shows a tremendous lack of data, as depicted in Fig. 19. The most notable difference here is that approximately one third of the C/E values are less than 0.1, with the vast majority of these being precisely zero due to missing reactions. This is not unexpected, since these libraries do not contain the data required for activation-transmutation simulations and should not be relied upon or trusted for such analysis. However, it is troublesome since it is often claimed that those libraries are validated for various applications that require these (and many other) reactions.

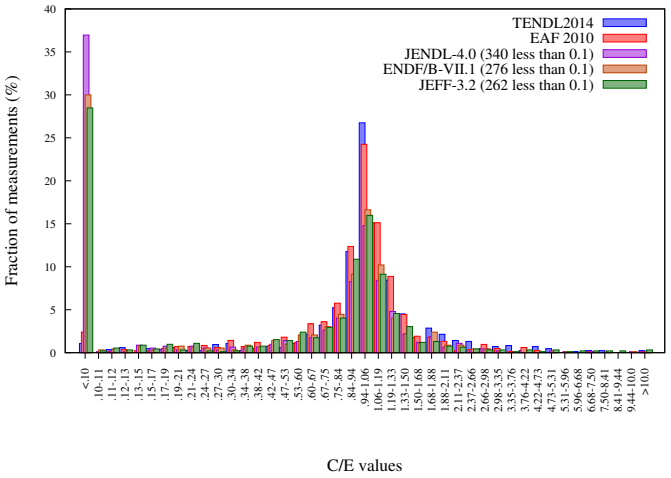

Figure 19: (Colour online) Distribution of integral measurement C/E values for TENDL-2014, EAF-2010, ENDF/B-VII.1, JENDL-4.0u and JEFF-3.2 neutron libraries. Note that values less than 0.1 also include zero, which is the case for around 1/3 in the legacy libraries.

4.3. Maxwellian-averaged cross sections

Many reaction channels have little or no experimental data, and for those with some measurements, these do not cover the full gambit of energies needed to properly describe the cross sections. In particular, the non-threshold reaction capture channels require a huge range of measurements to cover the resonance ranges, thermal values and high-energy components. Resonance parameters are typically generated with generalised least squares methods over a large, precise experimental database, but for most nuclides these are unavailable. In many cases not only are there not resolved resonance parameters, but very little or no integral data is available.

The importance of neutron capture and other non-threshold reactions for stellar nucleosynthesis processes has led experimentalists to measure integral cross sections for reactions which would otherwise have little attention. These are used to inform reaction rates in stellar nuclide evolution calculations which model the elemental composition of the observable universe. The importance of these values has led to the production of an evaluated reference database for Maxwellian-averaged cross sections: the Karlsruhe Astrophysical Database of Nucleosynthesis in Stars (KADoNiS) [58]. This contains data for 357 nuclides over a range of 11 temperatures form 5 keV (58 million K) to 100 keV (1.2 billion K). It draws largely upon the well-known compilation of Bao *et al.* [59], which includes an impressive catalogue of experimental and theoretical sources. While several of the nuclides without experimental information within Bao have been updated in the most recent KADoNiS database v0.3, 80 of these nuclides (22%) are based on theoretical, statistical model calculations rather than experimental measurements. Even though not as strong as the C/E validation for the remaining 277 nuclides, these

still provide code-to-code comparisons for the TENDL calculated values [60].

The TARES code of the TENDL generation system consistently produces the resonance parameters for the ENDF6 files `MF=2`, `MF=32` and `MF=33`, the last of which can be used with in the FISPACT-II uncertainty covariance collapse to generate specific rate uncertainties for each such non-threshold reaction channel. TARES also employs CALENDF resonance sampling methods [23] to statistically generate extended resolved resonance regions with enhanced capabilities for temperature-dependent broadening and self-shielding. These 'high-fidelity resonances' (HFR) [23] play a central role in the Maxwellian averaged values, particularly where no resonance data is available and step-function discontinuities between the low-energy region set by a thermal cross section and the higher-energy region can produce problematic temperature-dependent shapes. A prime example of this is shown in Fig. 20, where the TENDL HFR produces a more realistic cross section which produces a superior agreement with the KADoNiS values.

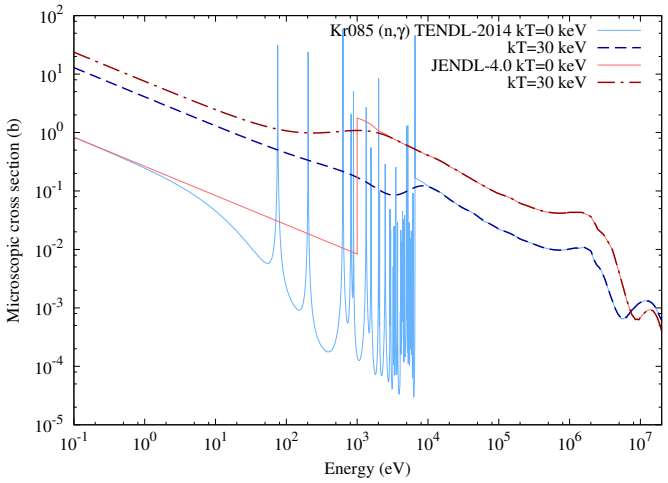

Figure 20: (Colour online) TENDL-2014 and JENDL-4.0u microscopic cross sections for Kr85, showing the unbroadened 0K and broadened 30 keV data. The TENDL-2014 C/E with KADoNiS is 0.92 at 30 keV.

A study of the MACS for all KADoNiS nuclides was performed using several methods, including the well known utility code `inter` [61], the JAEA `maxwav` [62] and FISPACT-II collapses which offered the complete covariance uncertainty for each reaction. Of course, this is limited to files which possess a full `MF=33` file and only where they are meaningful, so that resonance range treatment is still not fully implemented for any library. However, for some examples the TENDL nominal and uncertainty values are due to TALYS calculations where the full uncertainty is already available in the 2014 release, for example in Cd106 as shown in Fig. 21. The ability to not only offer predictive capture cross sections, but also predict realistic uncertainty bounds which match beautifully with the experimental data is a unique feature of TENDL.

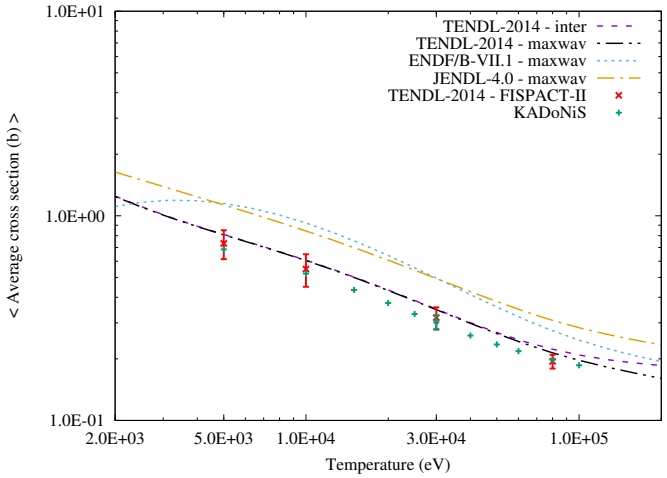

Figure 21: (Colour online) TENDL-2014, JENDL-4.0u and ENDF/B-VII.1 Maxwellian averaged cross sections for Cd106, showing the range of temperatures which cover the KADoNiS data points.

4.4. Fission decay heat

Decay heat and inventory calculations for irradiated fission fuels comprise two of the fundamental tasks for time-dependent Bateman solvers in the nuclear industry. Detailed and accurate knowledge of these time-dependent characteristics, as well as trustworthy uncertainty values, are of primary importance for reactor safety cases and the handling of irradiated fuel issues which cover a great many activities representing billions of dollars in current and future effort.

Development of the FISPACT-II code has resulted in new and unique simulation methods for a variety of nuclear observables, including fission decay heat and inventory calculations. To perform these simulations, massive libraries which contain the complete probability distributions for fission product formation, as well as the complete decay data for all of these products (reaching from the long-lived to those with sub-second half-lives), must be maintained and validated with sophisticated and sturdy simulation software. All of the physics of nuclear interactions, fissions and decays is contained within the nuclear data files, which hide one half of the simulation within the evaluation method behind those files.

While most time-dependent inventory and observables codes rely upon one bespoke nuclear data library, the ability to harness any dataset affords a unique opportunity to cross-check data and provide feedback which ultimately improves the code/data system. By performing a verification and validation on FISPACT-II with all of the major international nuclear data libraries, this exercise goes beyond demonstrating the capabilities of the code/data system in simulating decay heat and inventories, giving precise information on which nuclides should have their fission yield or decay data re-evaluated and in which library.

Table 8: Decay heat data sources with a primary author, experimental information and indicative year.

Author	Nuclide(s)	Method	Irrad. (s)
Fisher	$^{232}\mathrm{Th_f}$, $^{233}\mathrm{U_f}$, $^{235}\mathrm{U_f}$, $^{238}\mathrm{U_f}$, $^{239}\mathrm{Pu_f}$	γ	< 1
McNair	$^{235}\mathrm{U_{th}}$, $^{239}\mathrm{Pu_{th}}$	β	10–10^5
MacMahon	$^{235}\mathrm{U_{th}}$	β	10–10^4
Scobie	$^{235}\mathrm{U_{th}}$	β	10^4–10^5
Lott	$^{235}\mathrm{U_{th}}$	Total	100–5000
Yarnell	$^{233}\mathrm{U_{th}}$, $^{235}\mathrm{U_{th}}$, $^{239}\mathrm{Pu_{th}}$	Total	2×10^4
Jurney	$^{233}\mathrm{U_{th}}$, $^{235}\mathrm{U_{th}}$, $^{239}\mathrm{Pu_{th}}$	γ	2×10^4
Murphy	$^{235}\mathrm{U_f}$, $^{239}\mathrm{Pu_f}$	β	10^5
Dickens	$^{235}\mathrm{U_{th}}$, $^{239}\mathrm{Pu_{th}}$, $^{241}\mathrm{Pu_{th}}$	γ & β	1–100
Baumung	$^{235}\mathrm{U_{th}}$	Total	200
Akiyama	$^{233}\mathrm{U_f}$, $^{235}\mathrm{U_f}$, $^{238}\mathrm{U_f}$, $^{239}\mathrm{Pu_f}$	γ & β	10–300
Akiyama	$^{232}\mathrm{Th_f}$, $^{\mathrm{nat}}\mathrm{U_f}$	γ	10–300
Johansson	$^{235}\mathrm{U_{th}}$	γ & β	4–120
Tobias	$^{235}\mathrm{U_{th}}$, $^{239}\mathrm{Pu_{th}}$	Stat.	—
Schier	$^{235}\mathrm{U_{th}}$, $^{238}\mathrm{Pu_f}$, $^{239}\mathrm{Pu_{th}}$	γ & β	<1
Ohkawachi	$^{235}\mathrm{U_f}$, $^{237}\mathrm{Np_f}$	γ & β	10–300

4.4.1. Fission Experiments

To ensure that this validation [63] is as robust as possible, a thorough effort has been made to revisit as many high-quality decay heat experiments with complementary neutron spectra, irradiation schedules, measurement techniques and nations of origin. Simulations from theoretical fission bursts to full-day irradiations have been performed, using a variety of nuclear data combinations, and compared with the available experiments, which are summarised in Table 8. Good agreement between calculation and experiment (C/E) is found for total heat from the major fresh fuel components in actual LWRs, however spectroscopic partial heat and decay heat in thorium fuel cycle nuclides remains discrepant both in C/E and C/C. For minor actinides where no experimental data was available, C/C comparisons also show substantial differences between data libraries.

Detailed (spectroscopic and total) decay heat breakdown by nuclide is also performed for select cooling times and fissiles, using different decay or fission yield libraries to demonstrate the precise cause of the C/C discrepancies. These are found to primarily be due to incomplete adoption of TAGS results for Pandemonium nuclides, but many other decay data and fission yield differences have been identified. Given the tendency for relative agreement on total values, it is clear that many compensating effects are still present.

Thermal pulse experiments. A large set of thermal decay heat experiments have been performed for ^{235}U and ^{239}Pu, so that some statistical meta-analysis is necessary to handle the range of experimental values and uncertainties. While some chi-squared analysis may be proposed, the systematic issues with multiple experimental techniques, quality of campaigns and other factors must be taken into account. For these reasons, evaluated datasets have been produced, for example the Tobias evaluations or ANS/ANSI-5.1. Comparisons with predictions from FISPACT-II and other high-quality experiments show excellent agreement in total heat for all libraries, with some unresolved gamma/beta partial heat discrepancies due to TAGS data adoption.

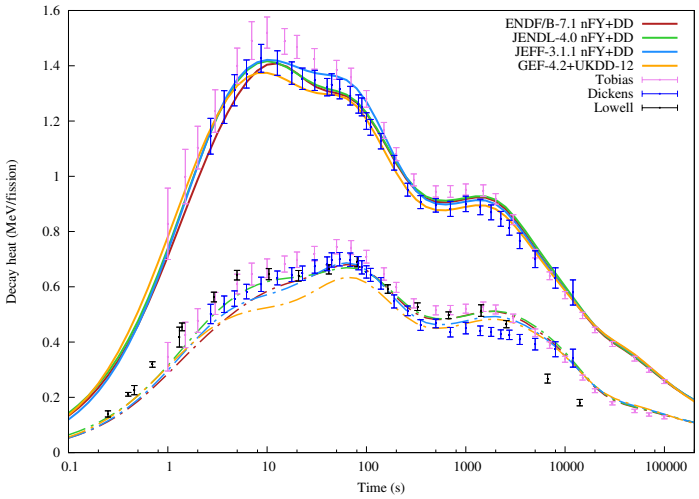

Figure 22: (Colour online) Total and gamma decay heat following thermal neutron pulse fission on ^{235}U, comparing well-known experimental data with FISPACT-II and all major libraries.

The remaining spectroscopic issues are largely related to the misallocation of gamma/beta energy in decay processes due to a lack of knowledge about beta decay feeding to high-energy excited daughter states. These low probability events are difficult to measure and consequently the average gamma energies are skewed downward, resulting in an incorrect apportionment of decay heat to the beta decay. Totals remain largely insensitive to the choice of decay library, but ENDF/B-VII.1 and JENDL-4.0u generally have more complete adoption of the most recent data which corrects these problems. As FISPACT-II has been engineered to accomodate any and all nuclear data, the user is able to choose to most appropriate physics based on the results of UKAEA validation.

Fast pulse experiments. The range of fast fission pulse experiments includes the Akiyama et al measurements using the YAYOI reactor for a variety of nuclides including ^{233}U, ^{235}U, ^{238}U, ^{239}Pu and ^{232}Th. These are complemented by UM Lowell data for ^{238}U and measurements of gamma heat from experiments using a Godiva device from Fisher

& Engle. Non-pulse fast measurements are also compared, for example from the UKAEA Zebra reactor.

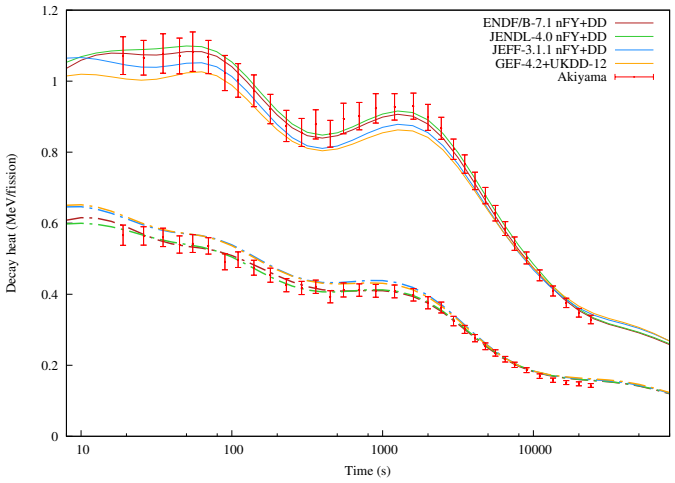

Figure 23: (Colour online) Total and beta decay heat following fast neutron pulse fission on ^{239}Pu, comparing well-known experimental data with FISPACT-II and all major libraries.

Except for some irregularities with the capture correction in the ^{232}Th gamma measurement, these are largely in agreement for all of the systems considered. Some differences were noted using previous GEFY-4.2 data which led to significantly different total heat predictions in short cooling times, typically less than 10 seconds. These in some cases are not within the scope of the available experiments to adequately probe and it should be noted that the GEF code has enjoyed significant and continued development in recent years and months. At present it is not the recommended library for typical thermal or fast reactor decay heat simulations, but its impressive capabilities make it the only option for many advanced applications and updated versions are continually in development and testing.

Finite duration experiments. Several non-pulse experiments were considered which employed a variety of neutron spectra, types/techniques, irradiation durations and cooling times. These vary from seconds to years post-irradiation (in some cases both in one experimental campaign), boil-off calorimetry to shielded gamma measurements and fast reactors to thermal columns. Quite importantly, they also include experiments from several countries and continents, including the UKAEA, LANL, Studsvik, CEA, ORNL, CENBG, Uppsala, KfK, SRRC and JAEA. Agreement with FISPACT-II predictions are generally very good, particularly better than the pulse cases where nuclides which suffer from the Pandemonium effect are less significant and numerous.

The example in Fig. 24 right shows a 100,000 second irradiation in the UKAEA Zebra reactor followed by beta heat measurements at a huge range of cooling times from

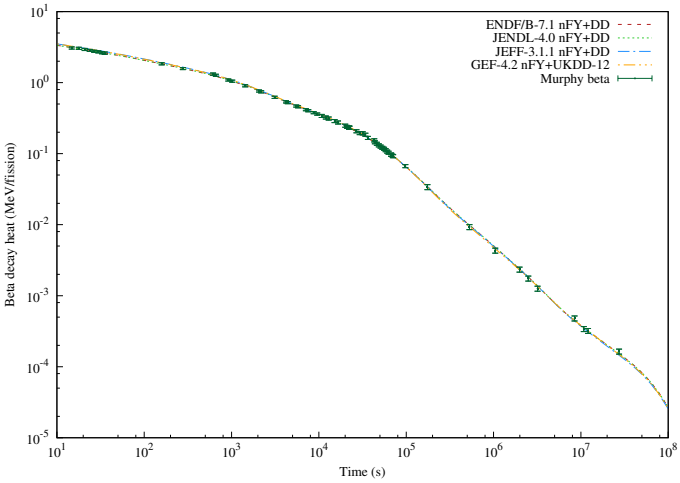

Figure 24: (Colour online) β decay heat following fast neutron irradiation for 10^5 seconds on ^{239}Pu at the UKAEA Zebra reactor, comparing experimental data with FISPACT-II and all major libraries.

just over ten seconds to nearly one year. The impressive agreement for all nuclear data libraries is in part attributable to the lower total number of nuclides with a significant role in a long (cumulative/equilibrium) irradiation.

4.4.2. Nuclear Data Probing

The use of different nuclear data libraries can have a profound effect on the simulation of decay heat for all fissile nuclides, including the main constituents of LWR fuel, for example. To better understand the root cause of these differences, FISPACT-II can be employed by swapping individual decay or fission files and comparing heat and inventories at a selection of cooling times. By doing this, the effects of library differences can be easily discovered and nuclides which both contribute non-negligibly to decay heat and have discrepant yields or decays can be identified.

The robust and open nature of the nuclear data functionalities of FISPACT-II allow it to follow all nuclides and precisely identify those nuclides which are responsible for discrepancies. For the nuclides which suffer from the Pandemonium effect, the beta heat is over-expressed due to mis-allocation of the heat due to high-energy gammas. This is not the only error possible with decay data files—misreading of data from ENSDF, dubious splitting of totals and simple typographical mistakes could also be at fault—but it is the most prevalent problem. To find the root cause, the decay data files must be interrogated by hand (ultimately by decay data evaluators). The example in Fig. 25 is the set of ^{233}U gamma heat contributors with nominal values on the left y-axis and ratios to the ENDF/B-VII.1 simulations on the right y-axis. In this comparisons JEFF-3.1.1 fission yields are exclusively used to ensure that any effects are solely due to the decay files. Note also the absence of ^{98}Zr gamma heat in all libraries

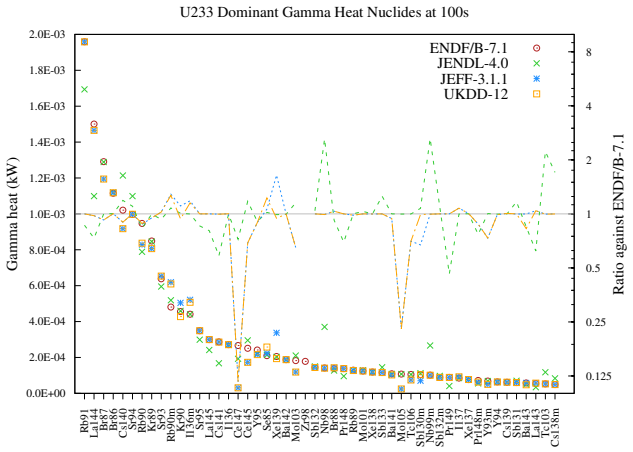

Figure 25: (Colour online) Comparison of the gamma heat at 100 s cooling following a fast neutron pulse on ^{233}U. Ratios are given on the right y-axis.

except ENDF/B-VII.1, which is due to files where only the ground state is populated in the beta decay.

Two supplements to the V&V report were prepared as compilations of nuclear data comparisons for general use; one with constant fission yields which compared the effects of varied decay data on decay heat [64] and another with constant decay data which tested fission yields [65].

4.5. Fission assembly simulations

As part of an international collaboration on uncertainty methods in reactor simulations [25], a set of reactor assemblies were modelled using CASMO-5 [66] with ENDF/B-VII.1 nuclear data. The neutron spectra for each fuel pin and volumetric power normalisation for some 50 steps of a 40 GWd/THM irradiation scenario were calculated by CASMO-5, providing the necessary input for FISPACT-II to follow the full inventory.

To accurately incorporate this data, consistent 586-group cross sections and probability tables were generated from and for ENDF/B-VII.1, including total energy-dependent kerma. The energy- and time-dependent self-shielding factors for each of the major reaction channels were employed, including fission and absorption for all actinides (see Fig. 3 for an example). ENDF/B-VII.1 independent fission yields for all available files and complete decay processes for all fission products were used in the simulation. To match the power normalisation of CASMO, the total reaction kerma for the full inventory was used to set a time-dependent neutron flux which was renormalised on a 10 hour time-step in order to maintain the constant power normalisation.[2]

[2]Since FISPACT-II has been designed to treat flux as constant during any time-step, this re-normalisation period was required to prevent the time-dependence of the flux from affecting the power normalisation.

One of the assemblies simulated, from Takahama-3 [67], has a lattice depiction in Fig. 26, including an array of burnable gadolinium poison rods and water-filled guide tubes. Average spectra for each pin, with material-specific probability table self-shielding factors, were used to follow the inventory and compare directly with the CASMO-5 predictions. The simulation results with FISPACT-II were notably in agreement with the CASMO predictions, with ^{235}U within 2% and ^{238}U within 0.5% at 45 GWd/THM burn-up, as shown in Figure 27. Similar agreement was found with the other assembly simulations of that collaboration [25].

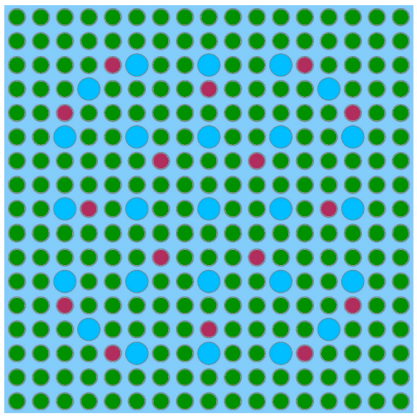

Figure 26: (Colour online) Takahama-3 assembly lattice with standard fuel rods (green), gadolinium rods (pink) and guide tubes (blue), as depicted by CASMO-5.

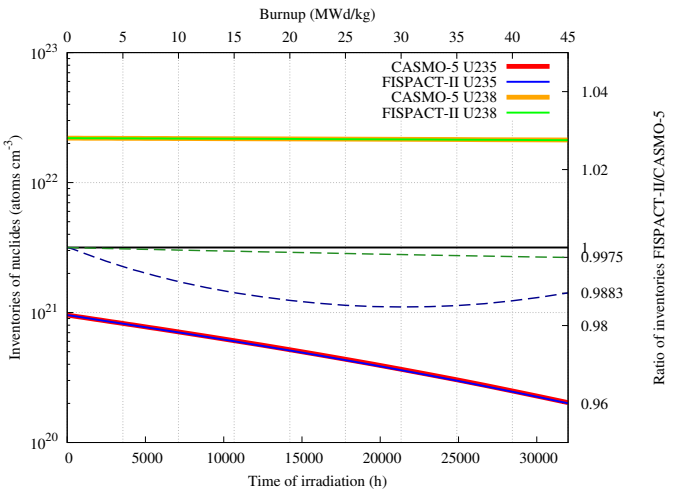

Figure 27: (Colour online) Takahama-3 assembly uranium inventories from CASMO-5 and FISPACT-II simulations over a 45 GWd/THM simulation. The ratio of ^{235}U (ending at 1.2% difference) and ^{238}U (ending at 0.25% difference) are also shown.

4.5.1. Total Monte-Carlo simulations

The ability to utilise arbitrary ENDF-6 formatted nuclear data files allows FISPACT-II to be naturally used in

Total Monte-Carlo uncertainty simulations, which implicitly include all nuclear data covariances that can be generated through parameter variation within the nuclear data generation codes. A novel Bayesian Monte-Carlo (BMC) method for fission yield uncertainty evaluation [26] using the GEF code [45] has been used to generate a set of fission yield files which represent the sampled GEF parameter distributions and resulting yield variations with full correlations. By sampling the random files in a set of otherwise-equivalent simulations, the uncertainties from the fission yields can be propagated. This has been employed to obtain fully-correlated fission yield uncertainties [68], for example with the ^{239}Pu pulse as shown in Fig. 28.

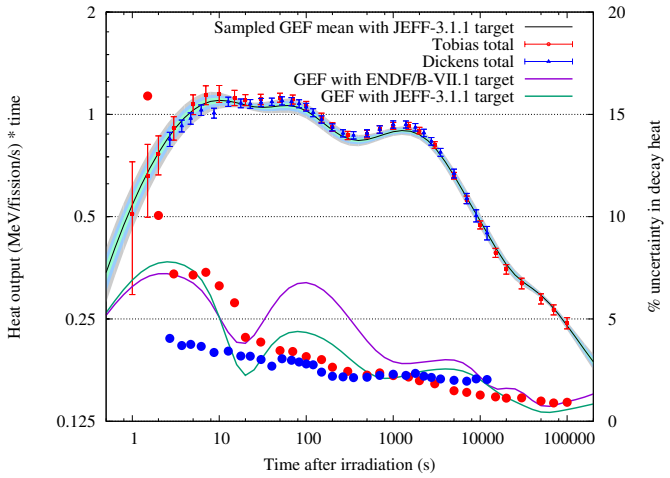

Figure 28: (Colour online) ^{239}Pu pulse decay heat simulations against experimental results from ORNL Dickens and the Tobias evaluation, using the BMC independent fission yields with JEFF-3.1.1 reference. The uncertainties from the ENDF/B-VII.1-based sampling are also compared with the experimentally-derived uncertainties.

In parallel, the pathways-based uncertainty from the energy-dependent covariance data for each reaction channel can be used to quantify the nuclear data uncertainty from the reaction cross sections. Combining the fission yield sampling with reaction covariance propagation provides a robust picture of these nuclear data uncertainties, as shown in the simulation of decay heat for the Takahama-3 assembly in Fig. 29. These reflect the full uncertainty propagation on all nuclides, including all major and minor actinides and approximately 1500 fission products from all fissiles actinides, as shown in Fig. 30.

5. Conclusions

The FISPACT-II system brings many new capabilities to the long established family of inventory codes. At the core of the main code is a rate equation solver that exploits the most advanced physics provided in modern nuclear data forms. This has primarily been driven by the

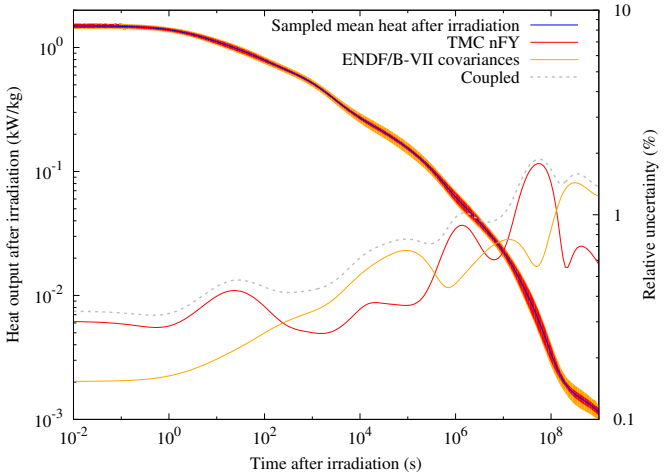

Figure 29: (Colour online) Takahama-3 SF97 after 45 MWd/THM using ENDF/B-VII.1 nuclear data for reaction covariances and BMC sampled fission yields for ^{235}U, ^{238}U, ^{239}Pu and ^{241}Pu.

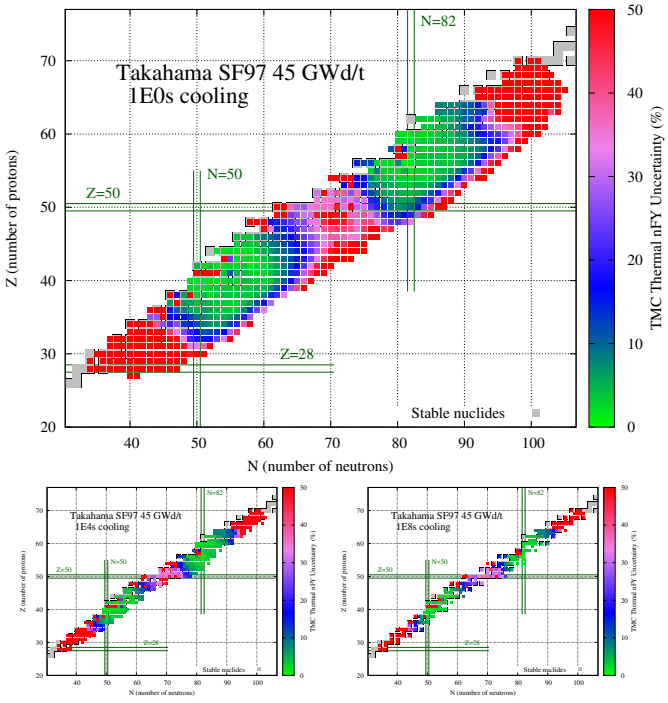

Figure 30: (Colour online) Takahama-3 SF97 after 45 MWd/THM using ENDF/B-VII.1 nuclear data for reaction covariances and BMC sampled fission yields, showing the propagated uncertainty for each of the fission yields simulated by FISPACT-II at cooling times of 1 second, 10^4 seconds (2.8 hours) and 10^8 seconds (3.2 years).

development of the technological TENDL nuclear data libraries that, when coupled with FISPACT-II, allow truly general-purpose simulations for neutron-induced inventory calculations, as well as a charged-particle simulations for proton, deuteron, alpha and gamma-ray irradiation.

The use of modern nuclear data forms opens up many novel features. New data forms for probability tables offer adaptable self-shielding calculations for a wide range of materials and irradiation scenarios, as well as geometry-specific self-shielding for several configurations. The inclusion of all reaction channels offers robust simulation of all inventory response functions, including damage source terms, gamma-dose, decay heat, activation-transmutation, depletion, gas production and kerma, dpa. These also provide new functionalities, such as the renormalisation of incident particle flux, through total or any partial kerma, to volumetric power rating. The availability of complete covariance data for all reaction channels, at least in TENDL, combined with the sophisticated pathways-based and Monte-Carlo sensitivity methods of FISPACT-II offers novel uncertainty quantification and propagation methods for all physical systems. The high-energy residual nuclide production data of TENDL, as read by FISPACT-II, allows fully tabulated nuclear data to be used in simulations of incident particles up to several hundred MeV.

Accessing all ENDF-6 nuclear data files, including both the well-known international libraries and the modern, technological files such as TENDL and GEFY has allowed FISPACT-II to be used to perform rigorous testing of the data against experimental values. These have verified the code capabilities, validated simulation results, uncertainty quantification and propagation methods and offered a new method for probing nuclear data files to find weaknesses when used for various applications.

With the new code functionalities, access to all general-purpose nuclear data and suite of modern V&V, FISPACT-II serves as a truly 21st software platform capable of leading the way safely and securely into the simulation needs of the present and future.

Acknowledgements

We would like to gratefully acknowledge the invaluable collaborations with A.J. Koning, D.A. Rochman, D.E. Cullen, R.E. MacFarlane and P. Ribon, J. Kopecky and R.A. Forrest, as well as their support, patience and advice over the years. They have paved the ways and we have followed with our own technologies and experience.

The FISPACT-II software was developed to meet UKAEA requirements in accord with modern software development standards. This work was done under contract by J.W. Eastwood and J.G. Morgan of Culham Electromagnetics Ltd., to whom special acknowledgement is due.

This work was funded by the RCUK Energy Programme under grant EP/1501045. To obtain further information on the data and models underlying this paper please contact PublicationsManager@ukaea.uk

References

[1] J.-C. Sublet, J. Eastwood, J. Morgan, M. Fleming, M. Gilbert, FISPACT-II User Manual, Tech. Rep. UKAEA-R(11)11 Issue 7, http://www.ccfe.ac.uk/fispact.aspx (Sep. 2015).

[2] R. Forrest, J.-C. Sublet, FISPACT-3: User Manual, Tech. Rep. AEA-FUS 227, AEA Technology, Culham Laboratory, aEA-Intec 1293 (April 1993).

[3] R. Forrest, J.-C. Sublet, EASY-97: a multipurpose activation and transmutation code system, Fusion Engineering, 17th IEEE/NPSS Symposium 1 (1997) 119 – 124.

[4] R. Forrest, FISPACT-2007: User Manual, Tech. Rep. UKAEA FUS 534, EURATOM/UKAEA Fusion Association (Mar. 2007).

[5] R. Burstall, FISPIN - A computer code for nuclide inventory calculations, Tech. Rep. ND-R-328(R), UKAEA (1979).

[6] J. Eastwood, J. Morgan, The FISPACT-II Software Specification Document, Tech. Rep. CEM/130516/SD/2 Issue 9, part of the FISPACT-II development documentation series available at http://culhamem.co.uk/fispact/ (Sep. 2015).

[7] K. Radhakrishnan, A. Hindmarsh, Description and use of LSODE, the Livermore solver for ordinary differential equations, Tech. Rep. LLNL Report UCRL-ID-113855, LLNL, `https://computation.llnl.gov/casc/odepack/odepack_home.html` (1993).

[8] O. Jarvis, Low-activity materials: reuse and disposal, Tech. Rep. AERE-R-10860, Atomic Energy Research Establishment (1983).

[9] H. Bateman, The Solution of a system of Differential Equations Occurring in the Theory of Radio-active Transformations, Proc. Camb. Phil. Soc. 16 (1910) 423.

[10] A. Hindmarsh, http://www.netlib.org/odepack/opkd-sum (2001).

[11] A. Hindmarsh, L. Petzold, A. Sherman, http://www.oecd-nea.org/tools/abstract/detail/USCD1229 (2005).

[12] J.-C. Sublet, P. Ribon, A Probability Table Based Cross Section Processing System: CALENDF - 2001, J. Nuc. Sci. Tech. Supplement 2 (2002) 856–859. `doi:10.1080/00223131.2002.10875233`.
URL `http://dx.doi.org/10.1080/00223131.2002.10875233`

[13] J.-C. Sublet, P. Ribon, M. Coste-Delclaux, CALENDF-2010: User Manual, Tech. Rep. CEA-R-6277, ISSN 0429-3460, CEA (2011).

[14] J.-C. Sublet, R. Blomquist, S. Goluoglu, R. Mac Farlane, Unresolved resonance range cross section probability and self shielding factors, Tech. Rep. CEA-R-6227, ISSN 0429-3460, CEA (2009).

[15] I. Bondarenko (Ed.), Group Constants for Nuclear Reactor Calculations, Consultant Bureau, New York, 1964.

[16] G. Bell, S. Glasstone, Nuclear Reactor Theory, Van Nostrand Reinhold, New York, 1970.

[17] V. Gopalakrishnan, S. Ganesan, Self-Shielding and Energy Dependence of Dilution Cross-Section in the Resolved Resonance Region, Ann. Nucl. Energy 25 (11) (1998) 839–857.

[18] E. Martinho, I. Gonçalves, J. Salgado, Universal curve of epithermal neutron resonance self-shielding factors in foils, wires and spheres, Appl. Radiation Isotopes 58 (3) (2003) 371–375.

[19] E. Martinho, J. Salgado, I. Gonçalves, Universal curve of the thermal neutron self-shielding factor in foils, wires, spheres and cylinders, J. Radioanal. Nucl. Chem. 261 (3) (2004) 637–643.

[20] J. Salgado, E. Martinho, I. Gonçalves, The calculation of neutron self-shielding factors of a group of isolated resonances, J. Radioanal. Nucl. Chem. 260 (2) (2004) 317–320.

[21] N. Baumann, Resonance integrals and self-shielding factors for detector foils, Tech. Rep. DP-817, du Pont de Nemours, Savannah River Laboratory (Jan. 1963).

[22] A. Koning, D. Rochman, Modern Nuclear Data Evaluation with the TALYS Code System, Nuclear Data Sheets 113 (12) (2012) 2841 – 2934, special Issue on Nuclear Reaction Data.

[23] D. Rochman, A. J. Koning, J. Kopecky, J.-Ch. Sublet, P. Ribon, M. Moxon, From average parameters to statistical resolved resonances, Annals of Nuclear Energy 51 (2013) 60–68.

[24] F. Fröhner, Evaluation and analysis of nuclear resonance data, Tech. rep., Nucear Energy Agency, jEFF Report 18 (2000).

[25] D. Rochman, O. Leray, M. Hursin, H. Ferroukhi, A. Vasiliev, A. Aures, F. Bostelmann, W. Zwermann, O. Cabellos, C. Diez, J. Dyrda, N. Garcia, E. Castro, S. van der Marck, H. Sjöstrand, A. Hernandez, M. Fleming, J. Sublet, L. Fioito, Nuclear Data Uncertainties for Typical Fuel Assemblies and a Simple Reactor Core, Nuclear Data Sheets X (XX) (2017) X – X.

[26] D. Rochman, O. Leray, A. Vasiliev, H. Ferroukhi, A. Koning, M. Fleming, J. Sublet, A bayesian monte carlo method for fission yield covariance information, Annals of Nuclear Energy 95 (2016) 125 – 134. doi:http://dx.doi.org/10.1016/j.anucene.2016.05.005.
URL http://www.sciencedirect.com/science/article/pii/S0306454916302511

[27] J. Eastwood, J. Morgan, J.-C. Sublet, Inventory uncertainty quantification using tendl covariance data in fispact-ii, Nuclear Data Sheets 123 (2015) 84 – 91, special Issue on International Workshop on Nuclear Data Covariances April 28 - May 1, 2014, Santa Fe, New Mexico, USA http://t2.lanl.gov/cw2014. doi:http://dx.doi.org/10.1016/j.nds.2014.12.015.
URL http://www.sciencedirect.com/science/article/pii/S0090375214006942

[28] M. R. Gilbert, J. Marian, J. -Ch. Sublet, Energy spectra of primary knock-on atoms under neutron irradiation, J. Nucl. Mater 467 (2015) 121–134. doi:10.1016/j.jnucmat.2015.09.023.

[29] R. E. MacFarlane, D. W. Muir, R. M. Boicourt, A. C. Kahler, The NJOY Nuclear data processing system – LA-UR-12-27079, http://t2.lanl.gov/nis/publications/NJOY2012.pdf (Version 2012-032).

[30] M. R. Gilbert, J.-Ch. Sublet, PKA distributions: Contributions from transmutation products and from radioactive decay, Nucl. Mater. EnergyIn press.

[31] M. Chadwick, M. Herman, P. Obloainske, M. Dunn, Y. Danon, A. Kahler, D. Smith, B. Pritychenko, G. Arbanas, R. Arcilla, R. Brewer, D. Brown, R. Capote, A. Carlson, Y. Cho, H. Derrien, K. Guber, G. Hale, S. Hoblit, S. Holloway, T. Johnson, T. Kawano, B. Kiedrowski, H. Kim, S. Kunieda, N. Larson, L. Leal, J. Lestone, R. Little, E. McCutchan, R. MacFarlane, M. MacInnes, C. Mattoon, R. McKnight, S. Mughabghab, G. Nobre, G. Palmiotti, A. Palumbo, M. Pigni, V. Pronyaev, R. Sayer, A. Sonzogni, N. Summers, P. Talou, I. Thompson, A. Trkov, R. Vogt, S. van der Marck, A. Wallner, M. White, D. Wiarda, P. Young, ENDF/B-VII.1 Nuclear Data for Science and Technology: Cross Sections, Covariances, Fission Product Yields and Decay Data , Nuclear Data Sheets 112 (12) (2011) 2887 – 2996, special Issue on ENDF/B-VII.1 Library. doi:http://dx.doi.org/10.1016/j.nds.2011.11.002.
URL http://www.sciencedirect.com/science/article/pii/S009037521100113X

[32] K. Shibata, O. Iwamoto, T. Nakagawa, N. IWAMOTO, A. ICHIHARA, S. KUNIEDA, S. CHIBA, K. FURUTAKA, N. OTUKA, T. OHASAWA, T. MURATA, H. MATSUNOBU, A. ZUKERAN, S. KAMADA, J.-i. KATAKURA, JENDL-4.0: A New Library for Nuclear Science and Engineering, Journal of Nuclear Science and Technology 48 (1) (2011) 1–30. arXiv:http://www.tandfonline.com/doi/pdf/10.1080/18811248.2011.9711675, doi:10.1080/18811248.2011.9711675.

[33] A. Koning, R. Forrest, M. Kellett, R. Mills, H. Henriksson, Y. Rugama, The JEFF-3.1 Nuclear Data Library, Tech. Rep. NEA No. 6190, OECD NEA (2006).

[34] A. Koning, et al., TENDL-2014: TALYS-based Evaluated Nuclear Data Library, http://www.talys.eu/tendl-2014 (2014).

[35] A. Koning, S. Hilaire, S. Goriely, TALYS-1.7, User Manual, Nuclear Research and Consultancy Group NRG, Petten.

[36] K.-H. Schmidt, B. Jurado, C. Amouroux, General view on nuclear fission (2014) 1–208arXiv:http://hal.in2p3.fr/file/index/docid/976648/filename/GEF.pdf.

[37] K.-H. Schmidt, GEFY: GEF-based fission-fragment Yield library in ENDF format, www.khs-erzhausen.de/GEFY.html (2015).

[38] R. A. Forrest, The European Activation File: EAF-2007 decay data library, Tech. Rep. UKAEA FUS 537, EURATOM/CCFE (2007).

[39] A. Hodgson, R. Grimes, M. Rushton, O. Masden, The impact of neutron cross section group structures on the accuracy of radiological source models, Nuclear Science and Engineering 181 (3) (2015) 1–8, http://dx.doi.org/10.13182/NSE14-156.

[40] M. Fleming, L. Morgan, E. Shwageraus, Optimisation algorithms for multi-group energy structures, Nuclear Science and Engineering 183 (2) (2016) 179–184, http://dx.doi.org/10.13182/NSE15-55.

[41] NEA, The JEFF-3.1/-3.1.1 Radioactive Decay Data and Fission Yields Sub-libraries, JEFF Report 20 (2009).

[42] OECD NEA, The JEFF-2.2 Radioactive Decay Data, OECD NEA, JEFF Report 13 (1994).

[43] E. Brown, R. Firestone, Table of Radioactive Isotopes, John Wiley and Sons, 1996.

[44] L. Packer, J.-C. Sublet, The European Activation File: EAF-2010 decay data library, Tech. Rep. CCFE-R(10)02, CCFE (2010).

[45] K.-H. Schmidt, B. Jurado, C. Amouroux, C. Schmitt, Special issue on nuclear reaction data general description of fission observables: Gef model code, Nuclear Data Sheets 131 (2016) 107 – 221. doi:http://dx.doi.org/10.1016/j.nds.2015.12.009.
URL http://www.sciencedirect.com/science/article/pii/S0090375215000745

[46] C. Jouanne, J.-Ch. Sublet, TRIPOLI-4.4 JEFF-3.1 Based Libraries, Tech. Rep. CEA-R-6125, ISSN 0429-3460, CEA (2006).

[47] J. C. Sublet, JEFF-3.1, ENDF/B-VII and JENDL-3.3 Critical Assemblies Benchmarking With the Monte Carlo Code TRIPOLI, IEEE Transactions on Nuclear Science 55 (1) (2008) 604–613. doi:10.1109/TNS.2007.911600.

[48] J. M. Ruggieri, et Al., ERANOS 2.1:International Code System for GEN IV Fast Reactor Analysis, International Congress on Advances in Nuclear Power Plants (ICAPP 2006)http://www.ans.org/store/item-700324-CD/.

[49] J.-Ch. Sublet, C. Dean, D. Plisson-Rieunier, ECCOLIB-JEFF-3.1 Based Libraries, Tech. Rep. CEA-R-6100, ISSN 0429-3460, CEA (2006).

[50] F. Maekawa, et al., Compilation of benchmark results for fusion related nuclear data, Tech. Rep. JAERI-Data/Code 98-024, JAEA, http://www.jaea.go.jp/jaeri/ (1998).

[51] F. Maekawa, et al., Data collection of fusion neutronics benchmarking experiment conducted at FNS/ JAERI, Tech. Rep. JAERI-Data/Code 98-021, JAEA, http://www.jaea.go.jp/-jaeri/ (1998).

[52] F. Maekawa, M. Wada, Y. Ikeda, Decay Heat Experiment and Validation of calculation code systems for fusion reactor, Tech. Rep. JAERI 99-055, JAEA, http://www.jaea.go.jp/jaeri/ (1999).

[53] J.-C. Sublet, M. Gilbert, Decay heat validation, FISPACT-II&TENDL-2015, JEFF-3.3, ENDF/B-VII.1 and JENDL-4.0 nuclear data libraries, Tech. Rep. UKAEA-R(16)36, UKAEA, http://www.ccfe.ac.uk/fispact.aspx/ (2016).

[54] J.-Ch. Sublet, M. Gilbert, Decay heat validation, FISPACT-II & TENDL-2014, JEFF-3.2, ENDF/B-VII.1 and JENDL-4.0 nuclear data libraries, Tech. Rep. CCFE-R(15)25, CCFE, http://www.ccfe.ac.uk/FISPACT.aspx (2015).

[55] N. Otuka, E. Dupont, V. Semkova, B. Pritychenko, A. Blokhin, M. Aikawa, S. Babykina, M. Bossant, G. Chen, S. Dunaeva, et al., Towards a more complete and accurate experimental nuclear reaction data library (EXFOR): international collaboration between nuclear reaction data centres (NRDC), Nuclear Data Sheets 120 (2014) 272–276.

[56] M. Fleming, J.-Ch. Sublet, J. Kopecky, Integro-differential Verification and Validation, FISPACT-II & TENDL-2014 nuclear data libraries, Tech. Rep. CCFE-R(15)27, CCFE (2015).

[57] J.-Ch. Sublet, G. J. Butterworth, Fusion Activation of Ferrous Alloys, Fus. Eng. Des. 22 (1993) 279–321.

[58] I. Dillmann, M. Heil, F. Käppeler, T. Rauscher, KADoNiS v0.3

- The third update of the Karlsruhe Astrophysical Database of Nucleosynthesis in Stars, in: Proceeding of the workshop EFNUDAT Fast Neutrons - scientific workshop on neutron measurements, theory and applications, Geel, Belgium, 2009.

[59] Z. Bao, H. Beer, F. Käppeler, F. Voss, K. Wisshak, T. Rauscher, Neutron Cross Sections for Nucleosynthesis Studies, Atomic Data and Nuclear Data Tables 76 (1) (2000) 70 – 154. doi:http://dx.doi.org/10.1006/adnd.2000.0838.
URL http://www.sciencedirect.com/science/article/pii/S0092640X00908386

[60] J.-Ch. Sublet, M. Fleming, Maxwellian-Averaged Neutron-Induced Cross Sections for kT=1 keV to 100 keV, KADoNiS, TENDL-2014, ENDF/B-VII.1 and JENDL-4.0u nuclear data libraries, Tech. Rep. UKAEA-R(15)29, UKAEA, http://www.ccfe.ac.uk/FISPACT.aspx (March 2015).

[61] C. Dunford, A. Trkov, ENDF Utility Codes version 7.02-8.2, http://www.nndc.bnl.gov/nndcscr/endf/endf-util/index.html.

[62] K. Shibata, Private communication (December 2014).

[63] M. Fleming, J.-Ch. Sublet, Validation of FISPACT-II decay heat and inventory predictions for fission events, Tech. Rep. CCFE-R(15)28, CCFE (2015).

[64] M. Fleming, J.-Ch. Sublet, Decay datacomparisons for decay heat and inventory simulations of fission events, Tech. Rep. CCFE-R(15)28/S1, CCFE (2015).

[65] M. Fleming, J.-Ch. Sublet, Fission yield comparisons for decay heat and inventory simulations of fission events, Tech. Rep. CCFE-R(15)28/S2, CCFE (2015).

[66] J. Rhodes, K. Smith, D. Lee, CASMO-5 development and application, in: PHYSOR-2006, ANS Topical Meeting on Reactor Physics, Canadian Nuclear Society, Vancouver, BC, Canada, 2006.

[67] C. Sanders, L. Gauld, Isotopic analysis of high-burnup PWR spent fuel samples from the Takahama-3 reactor, Tech. Rep. NUREG/CR-6798, ORNL/TM-2001/259, Oak Ridge National Laboratory (2003).

[68] O. Leray, D. Rochman, M. Fleming, J. Sublet, A. Koning, A. Vasiliev, H. Ferroukhi, Fission yield covariances for JEFF: a Bayesian Monte Carlo method, in: ND 2016 International Conference on Nuclear Data for Science and Technology, 2016.